



AirCargoChallenge 2022

Technical Report

Team #23

U-Fly Aerodesign



Table of Contents

Abbreviations	1	Dynamic stability.....	17
INTRODUCTION.....	3	Control surfaces	17
PROJECT MANAGEMENT.....	3	Aileron sizing.....	17
Project Work Distribution	3	Elevator sizing	18
Competition Requirements.....	4	Rudder sizing.....	18
Design decisions.....	4	STRUCTURAL DESIGN.....	18
Team’s general purpose.....	4	Payload placement	19
Conceptual design.....	4	Fuselage	19
Aircraft weight build-up methodology	5	Stress analysis	20
Wheel of Design	5	Main beam	20
Budget	6	Wing.....	20
Roadblocks	6	Landing gear.....	22
Failure Modes and Effects Analysis (FMEA).....	7	PERFORMANCE AND ELECTRICAL PROJECT	23
Gantt Chart.....	8	Propulsion model.....	23
AERODYNAMICS.....	9	Available vs. Required Power and Thrust	24
Design Goals.....	9	Take-off total mass and take-off distance	24
Wing position	9	Rate-Of-Climb	25
Constrains diagram	9	Turning Rate.....	25
Airfoil selection, positioning and testing	9	Flight Time and Range	25
Geometry selection.....	11	Flight envelope	26
High-lift device	12	Servomotors	26
CFD analysis.....	13	Batteries selection	27
Lift Distribution	13	Aircraft’s electrical model.....	27
Drag polar.....	14	PAYLOAD PREDICTION	27
STABILITY AND CONTROL.....	14	28
Airfoil selection	14	MANUFACTURING PROCESS.....	28
Tail sizing	15	OUTLOOK	29
Gravity center, neutral point, and static margin ...	16	REFERENCES.....	30
Longitudinal and lateral-directional static stability and control.....	16		

Abbreviations

ah	Rotation angle of the control surface	m	Mass
AHP	Analytic Hierarchy Process	m_a	Aircraft mass
AR	Aspect ratio	MAC	Mean aerodynamic chord
as	Rotation angle of the servo arm.	M	Bending moment

b_R	Rudder span	ME	Static margin
b_V	Vertical tail wingspan	m_L	Payload mass
b_w	Wingspan	$MTOW$	Maximum take-off weight
c	Wing chord	n	Load factor
c_r	Root chord	N	Normal force
c_t	Tip chord	n_{bp}	Security factor for battery estimation
C_D	Drag coefficient	n_{max}	Maximum load factor
$C_{D_{TO}}$	Take-off drag coefficient	n_{Rmin}	Load factor for minimum turning radius
CG	Center of gravity	n_{ult}	Ultimate load factor
C_{HT}	Horizontal tail volume coefficient	P	Roll rate
C_L	Lift coefficient	p	roll rate
C_{L_h}	Tail lift coefficient	q	pitch rate
$C_{l_{max}}$	Airfoil maximum lift coefficient	q_{bp}	Minimum battery capacity
C_{l_p}	Roll damping coefficient	QFD	Quality Function Deployment
$C_{L_{TO}}$	Take-off lift coefficient	r	yaw rate
C_{L_α}	Lift coefficient due to angle of attack	R	Universal gas constant
$C_{L_{\alpha_h}}$	Horizontal tail lift curve slope	ROC	Rate-Of-Climb
$C_{L_{\alpha_V}}$	Vertical tail lift curve slope	$R_{turn_{min}}$	Minimum turning rate
$C_{l\delta\alpha}$	Aircraft rolling moment due to aileron deflection.	S_G	Take-off distance
C_m	Moment coefficient	S_w	Wing area
C_{m_α}	Moment coefficient due to angle of attack	t_{min}	Minimum flight time
$C_{n\delta R}$	Rudder yaw control power	T_0	Temperature at sea level
$C_{rating, bp}$	Minimum battery C-rating	TR	Taper ratio
C_{VT}	Vertical tail volume coefficient	u	Velocity along X body axis
C_w	Wing mean chord	UAV	Unmanned Aerial Vehicle
D	Drag	v	velocity along Y body axis
e	Oswald's efficiency	V	Aircraft speed
FEM	Finite Element Method	V_{Rmin}	Minimum turning radius airspeed
F_s	Safety factor	V_{TO}	Take-off speed
g	Acceleration due to gravity	\bar{V}_V	Vertical tail volume coefficient
I	Moment of inertia	w	velocity along Z body axis
I_{max}	Maximum motor current	W_i	Aircraft weight
L	Surface length	X_{CG}	Center of gravity along x axis
L_{HT}	Horizontal stabilizer's aerodynamic center to wing's aerodynamic center moment arm	X_{NP}	Neutral point
L_{VT}	Vertical stabilizer's aerodynamic center to wing's aerodynamic center moment arm	z	Altitude
α	Angle of attack	$\lambda_{c/2}$	Sweep angle at mid-chord
α_h	Elevator operational angle of attack	μ	Friction coefficient
γ	Climb angle	ρ	Air density
δ_E	Elevator deflection	σ_{max}	Maximum bending stress

η_V	Vertical tail dynamic pressure ratio	τ_e	Angle of attack effectiveness of the elevator
θ	pitch angle	τ_r	Rudder angle of attack effectiveness
λ	Altitude-temperature relation in the Troposphere	ϕ	Bank angle

INTRODUCTION

This report specifies the participation of U-Fly Aerodesign team in Air Cargo Challenge 2022 competition on behalf of the Universidad Aeronáutica en Querétaro (UNAQ) from Mexico. Herein, an overview of the aircraft design process and its performance expectations is provided.

After the COVID 19 pandemic, humanity’s perception of the healthcare sector shifted dramatically. Nowadays, aerial drone technology is being used to improve the quality of life in rural areas by decreasing lab test turnaround times, enabling just-in-time delivery of supplies and medical devices by reducing the costs of routine prescription drugs.

Understanding the regulatory limitations, U-Fly set out to design an aircraft capable of transporting a set amount of blood bags arranged within a cargo bay, being able to take off and land in a short distance through challenging terrain. The entire aircraft must be able to be transported and assembled within the dimensional limits imposed by the competition, whilst performing adequately and effectively a valid flight circuit under power limitations. These considerations culminated in “Zotz”, or bat in Mayan, whose name comes from the aircraft's primary function of carrying blood bags; so, a blood-sucking, flying, animal species with a significant role in the cosmogony of our region was selected.

Zotz is cargo aircraft, able to contain 2.4kg in blood bags in its payload boxes within the internal structure of the wing and the fuselage. Its span is 2.166m long, with a surface of 0.57m², and it’s the first aircraft developed by the team that uses flaps. It has a twin tail configuration and uses the specified motor AXI2826/10 Gold Line V2 with a propeller APC 10X6E. Its cruising speed of 18m/s is a match with the drag reduction that the aircraft had to endure to be what it is presented in the next pages. The bat is strongly associated with blood and has an intrinsic relationship with life, and it is precisely what we want to guarantee, life. U-Fly accepted the challenge and designed an aircraft to fulfill those expectations.

PROJECT MANAGEMENT

Project Work Distribution

Throughout its history, U-Fly Aerodesign team has been characterized for developing innovative solutions that meet the specific purposes of each competition based on a deep commitment to a philosophy of union and communication among its members. To achieve this, the team is divided into five working areas, the responsibilities of each one during the Zotz project are described below.

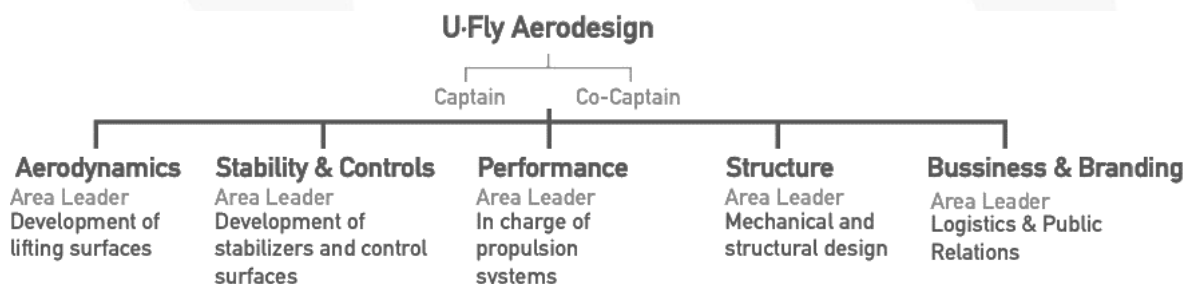


Figure 1. Work distribution.

Competition Requirements

From the competition's regulations document, the team formulated the requirements that the aircraft should comply with:

- The aircraft must fit into a transport box, this must not exceed 1.1m x 0.4m x 0.25m
- The size of the "ready-to-fly" aircraft must fit in a diamond-shaped box with an edge length of 1.5 m each; the angle between the edges is not fixed and has a maximum height of 0.5 m.
- The payload must be enclosed within the aircraft structure, fixed in one position on the aircraft.
- The maximum take-off distance should be 60m, to get extra bonus points the maximum take-off distance should be 40m; the landing field is made of grass.
- The cargo bay must accommodate at least one blood bag with 300g.
- Aircraft's assembly time must be less than 60 min.
- Guarantee the integrity of the electronic components of the aircraft in various weather conditions.
- The aircraft should reach 100 m in less than 60 seconds (better lift at take-off).
- The aircraft should cover the greatest distance in 120 seconds.
- The aircraft manufacture should have a small budget
- The aircraft must withstand static wing deformation test (loads the aircraft from the tips).
- Aircraft's loading and unloading time less than 120s.
- Use of a Unilog GPS Logger 3 screwed to the aircraft with two M3 to avoid steep tilt angles ($>40^\circ$) and high G-loads ($>3-4g$).
- The aircraft should fly in a range between 10m and 120m altitude.

Design decisions

After reading and discussing the regulation requirements the team took the following design decisions, where one of the goals was to assure that the aircraft will have a valid flight at least 66% of the rounds.

- Consider reducing drag on the aircraft design.
- Use the volume on the wing to carry payload in order to reduce the fuselage size and thus the drag.
- Consider the correlation between distance and speed during cruise flight.
- Carry the largest payload safely within our design constraints and considering the score analysis.
- Assure a safe static margin at different payloads.
- Choose the wing configuration considering the best lift distribution.
- Locate the data logger in a safe place and a stable lateral and longitudinal position.
- Accomplish a safe take-off distance of 40m.
- Obtain the best possible performance with the propulsion system given in the regulations.

Team's general purpose

Design, justify, manufacture, and test a remotely piloted aircraft, easy to assemble, with a maximum takeoff distance of 40 meters, that transports the greatest possible payload, that achieves the maximum reachable distance in 120 seconds, and all within a small budget.

Conceptual design

To achieve the concept of the aircraft, U-Fly Aerodesign's flight mission was to find a balance between the largest payload and the highest achievable speed, keeping stability and safety while performing the flight pattern given by the competition's regulations. We aimed to design and manufacture an aircraft that could be easily assembled and would meet all the design decisions stated above, where each of the working areas should address the challenges of their concern.

The wing with the best aerodynamic performance was an elliptic geometric configuration, thus because the difficulty in manufacturing a Schuemann geometry was chosen because it reduced drag. After analyzing

several cargo and non-cargo airfoils, it was decided to use a non-cargo airfoil to reduce drag, rather than use a cargo airfoil to increase lift but increase drag too. Because of that decision the teams decided to include a high lift surface to increase lift at critical moments such as takeoff.

Due to space requirements and a to assure the stability and integrity of the aircraft a twin tail (U-tail) empennage was implemented, since it has two vertical stabilizers the working area is less and provides good stability.

As of the measurement system, a compartment was allocated in the upper part of the aircraft. Finally, to reduce drag and make the most of the structure's space, three cargo bays were distributed throughout the aircraft, two inside the wing and one below; the last one also supports the landing gear and places the electronic components in a safe space as close as possible to the engine.

Aircraft weight build-up methodology

The total mass of the aircraft was calculated by adding the main component's mass. The fuselage, leading edges, PTR and empennage masses were obtained from its preliminary CAD models.

TOTAL MASS							
Component	Mass (g)	Component	Mass (g)	Component	Mass (g)	Component	Mass (g)
Wing	700	Main landing gear	116	Left aileron servo	15.8	Motor	177
Horizontal stabilizer	75	Main battery	250	Right aileron servo	15.8	Logger	150
Vertical stabilizer 1	13.92	Secondary battery	63.3	Flap servo	26	Shunt Plug	70
Vertical stabilizer 2	13.92	Elevator servo	26	Nose landing gear servo	26	Fixing Motor-PTR	4.07
Fuselage	215.2	Left rudder servo	13	ESC- Speed Controller	70	Receiver	9.3
Nose gear	63.58	Right rudder servo	13	Propeller	27	PTR	150
Total Mass (g)						2303.89	

Table 1. Total mass estimation table.

Wheel of Design

The development of the project was conducted following the strategy proposed by Daniel P. Raymer's "Wheel of Design" [1], which acknowledges four main stages: requirements, conceptual design, design analysis, and flight test.

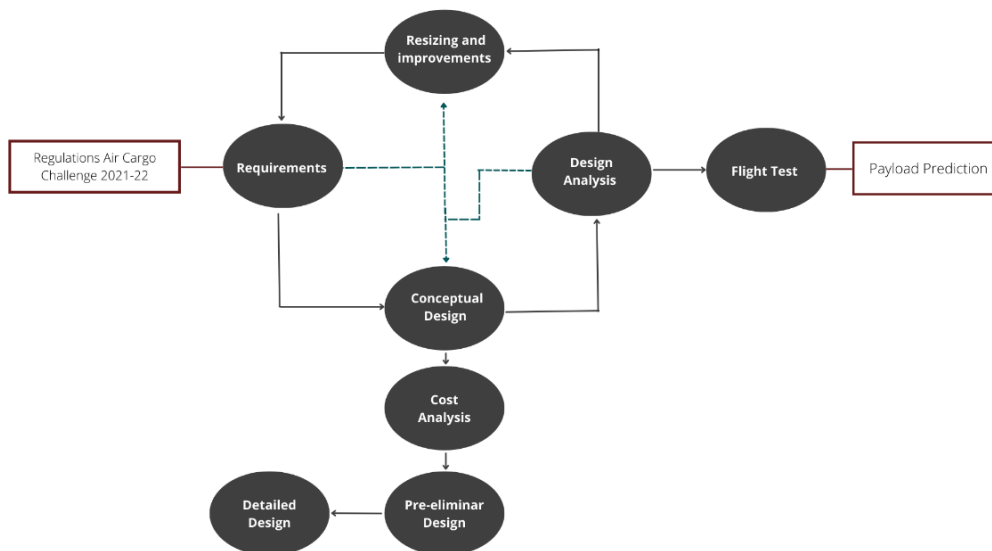


Figure 2. Wheel of Design.

analysis, and resizing and improvements. There is a correlation among them where, simultaneously, work is done on aspects that encompass more than one category, which entails high communication among areas.

As a starting point and based on the regulations, an internal brainstorming was executed in each area to develop the conceptual design. Later, the analysis for the preliminary design was carried out by unifying proposals. Finally, it was detailed through simulations and flight tests that provide arguments to modify or improve the project.

Budget

For the administration of team resources, a cost analysis was completed in table 2, describing the total cost for an aircraft broken down by areas. For the project to be viable, the team had the support of our alma mater, the Aeronautical University in Querétaro (UNAQ); and various companies, which provided materials, use of machinery, and tools at no cost. In addition, table 3 shows the estimate of economic resources to fulfill the Air Cargo Challenge 2021-22 competition considering the manufacture of two aircraft and a travel budget.

Budget for Aircraft	
Primary aircraft electrical system	\$ 222.70
Electrical surface control system	\$ 437.46
Wing's composite materials	\$ 139.96
Tail's composite materials	\$ 351.38
Fuselage's composite materials	\$ 129.60
Wing's woods	\$ 44.65
Tail's woods	\$ 44.65
Fuselage's woods	\$ 15.45
Laser cutting	\$ 45.54
Supplies	\$ 86.92
Screws	\$ 35.21
MonoKote covering film	\$ 16.99
Landing gear	\$ 30.00
TOTAL	\$ 1,600.51

Table 2. Budget for aircraft.

General Budget	
Aircrafts	\$ 4,801.52
Flights	\$ 11,180.00
Transport	\$ 2,393.70
Application fees	\$ 2,980.00
Hotel	\$ 2,026.40
Meals	\$ 2,690.00
TOTAL	\$ 26,071.62

Table 3. General budget.

Roadblocks

Due to the pandemic, adjustments took place in the way the team used to work, conducive to the adaption of reality never experienced. Many barriers predisposed us to not being able to make significant progress at first. Face-to-face meetings were unimaginable until a few months ago. The limitation of a closed university took away all our tools and material available and added uncertainty that distanced us from the objective.

On the other hand, the journey throughout the competition was full of learning. Because of our background in utility aircraft design competitions, the team had the challenge of designing its first heavy-less and fast aircraft. Hence, implementations (accompanied by research) happened in every area, aspiring to achieve the most optimum design overall. For stability and control, their focus was reducing weight, which led to problems selecting the material, airfoils, and configuration for the empennage. Structures faced the challenge of space restriction in contrast to the weight and volume loaded without altering the gravity center. Components were constantly changed, seeking to reduce drag as much as possible. Aerodynamics sought an airfoil thick enough to contain the cargo bay, and, for the first time, a flap was executed in a structure assembled in three parts. Additionally, the Performance area had to be coupled to a specific engine (smaller than the ones used in SAE Mexico) which, together with the time and distance of the mission's ascent, were obstacles to overcome. Finally, the business area had difficulties importing materials from Europe.

The issues mentioned above continue to be challenging, but if there is something that characterizes the team is its perseverance that helps us translate the challenges into areas of opportunity to continue working as a team and ultimately grow.

Failure Modes and Effects Analysis (FMEA)

To discover potential failures that may exist within the process, a FMEA was formulated. Within, we considered the points that could affect the integrity and safety of the aircraft in flight catastrophically or dangerously, as shown in table 3. This way, we prioritized the mitigation of possible failures in addition to a correction proposed before the event occurred. For this occasion, the empty spaces of the "Actions Taken" column represent the actions that has not taken place and that are part of the manufacturing process that has not happened.

Process / Product Name		Design and manufacture process of "Zotz"		Prepared By		U-Fly Aerodesign								
Responsible		U-Fly Aerodesign		FMEA Date (Original)		04-04-22		Revised		Assitant teacher				
Process Step/Input	Potential Failure Mode	Potential Failure Effects	SEVERITY (1 - 10)	Potential Causes	Current Controls	DETECTION (1 - 10)	Risk Priority Number (RPN)	Action Recommended	Resp.	Actions Taken	SEVERITY (1 - 10)	OCURRENCE (1 - 10)	DETECTION (1 - 10)	Risk Priority Number (RPN)
What is the process step, change or feature under investigation?	In what ways could the step, change or feature go wrong?	What is the impact on the customer if this failure is not prevented or corrected?		What causes the step, change or feature to go wrong? (how could it occur?)	What controls exist that either prevent or detect the failure?			What are the recommended actions for reducing the occurrence of the cause or improving detection?	Who is responsible for making sure the actions are completed?	What actions were completed (and when) with respect to the RPN?				
Flaps design	Union of the structure with the servomotor	Lack of no deflection of the structure	9	Bad location of main frame or servo motor	Radio Control	7	378	Implement the review of the flap stroke in the checklist of the corresponding area	Aerodynamics and Performance					
	Error in aerodynamic analysis	Unreliable drag coefficients	10	Limitations of flap modeling in XFLR5 software	ANSYS CFX and XFLR5	4	320	Data comparison in ANSYS fluent	Aerodynamics	Wing analysis in ANSYS fluent	5	8	2	80
Reverse design of the airfoil	Interpolation failure at one or more points	Error in 3D modeling	9	XFLR5 software programming	No information	4	252	Previous analysis of the .txt file	Aerodynamics	Previous revision when entering SolidWorks of the coordinates of the profile	6	2	2	24
	Error in aerodynamic analysis	Unrepresentative data in 3D analysis	10	Little refinement of the wing geometry	Increased panels in geometry (XFLR5)	3	270	Increase of points in the profile interpolation	Aerodynamics	Increased wing geometry meshing	7	4	4	112
Propulsion and electrical system configuration	Insufficient power for flight	Aircraft crash	10	Lack of dynamic load testing	Ecalc, static tests and flight tests	3	90	Weight reduction of the aircraft or battery with greater capacity	Performance	Extensive analysis of available configurations before selection	6	1	2	12
	Selection of servo motors not suitable for aircraft mission	Loss or malfunction of stabilizing surfaces	10	Lack of torque	Static and dynamic tests	7	210	Change of servomotors without affecting the weight of the aircraft	Performance					
Selection of tires for landing gear	Poor performance of selected tires on grass	Possible structural loss of the aircraft on takeoff and landing	9	Poor impact resistance of selected tires	Dynamic tests	4	144	Comparative analysis of tires of different materials	Structures	Selection of rubber tires for landing gear	2	3	2	12
Preliminary empennage design	High static moment produced	Make the plane lan on its tail	4	Aircraft weight calculation error	Dynamic tests	1	20	Compensation with elements of the electrical and propulsive system at the front	Stability and Controls					

Table 4. FMEA table.

Gantt Chart

Since U-Fly Aerodesign is a high-performing student team, time management is indispensable. Based on a Gantt Chart, tasks were established starting from the regulation release date. The chart lists the activities carried out jointly and separately by area.

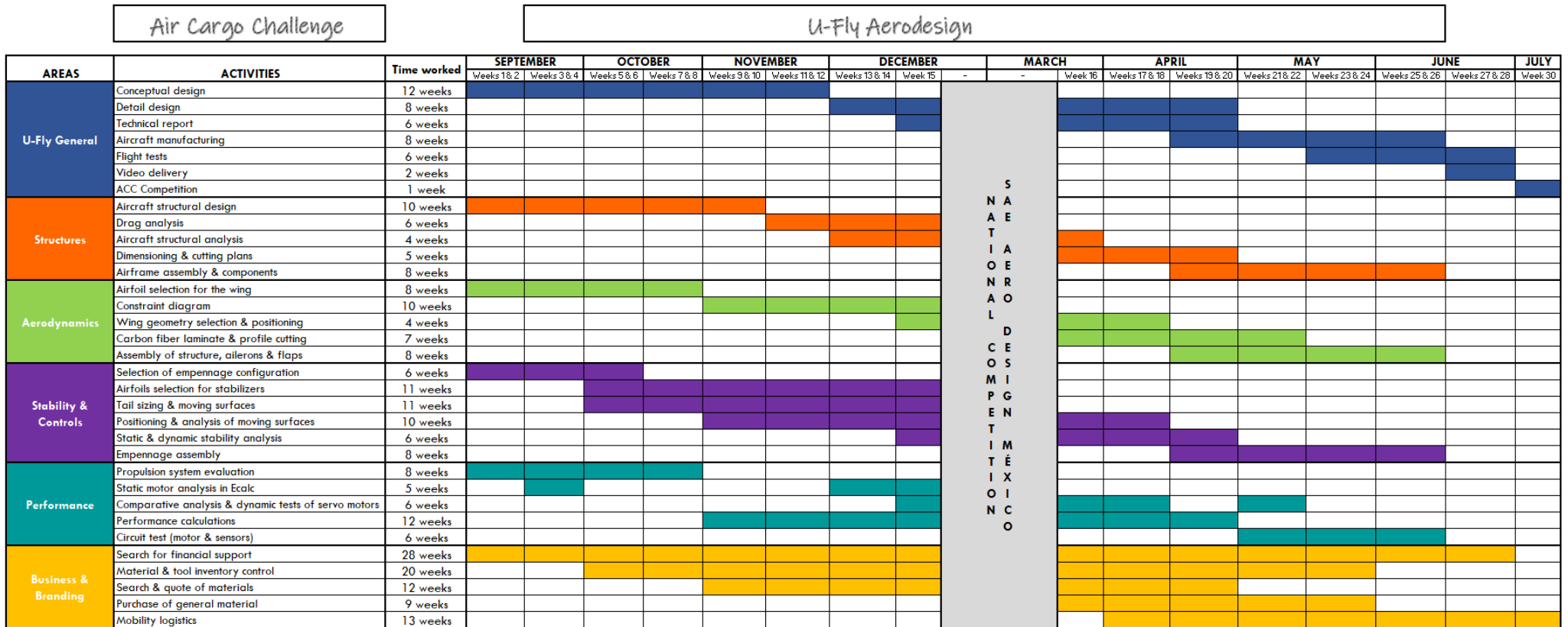


Figure 3. ACC 2022 Gantt Chart.

AERODYNAMICS

Design Goals

To design a wing, maximizing dimensions within the constraint box, that carries 1.8 kg within its structure, implementing high-lift devices to generate the required lift during take-off, and keeping drag as low as possible during cruise flight.

Wing position

Because the aircraft is cargo oriented, a high wing configuration was chosen to provide both good lateral stability and a cargo bay with enough volume. Also, this vertical positioning is attributed to help avoid possible damage to the wing integrity due to the runway characteristics and allows us to have an easier aircraft to assemble.

Constrains diagram

To obtain most flight round points, wing sizing was obtained using a MATLAB code based on Snorri Gudmundsson's initial dimensioning methodology [2]. Iterations were made considering Munich conditions, wing loading, cruise speed, and weight. A payload of 2.26 kg (see figure 4) and wing surface of 0.56 m² (see figure 5) were obtained as the optimal design point, with a cruising speed of 25.7 [m/s] and a wing loading of 74.69 [N/m²].

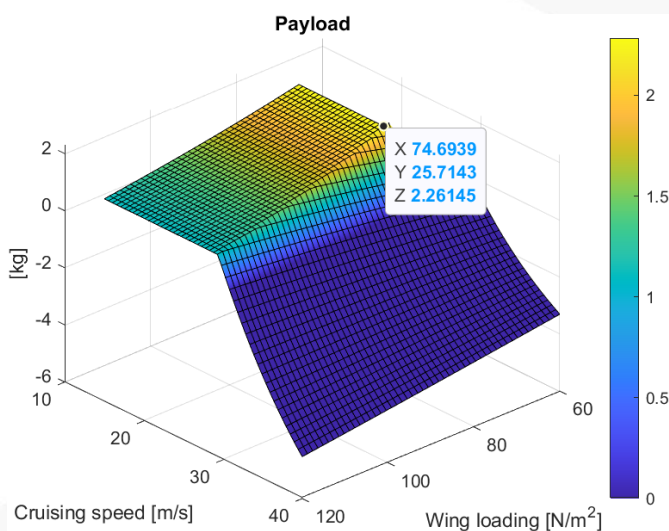


Figure 5. Payload diagram.

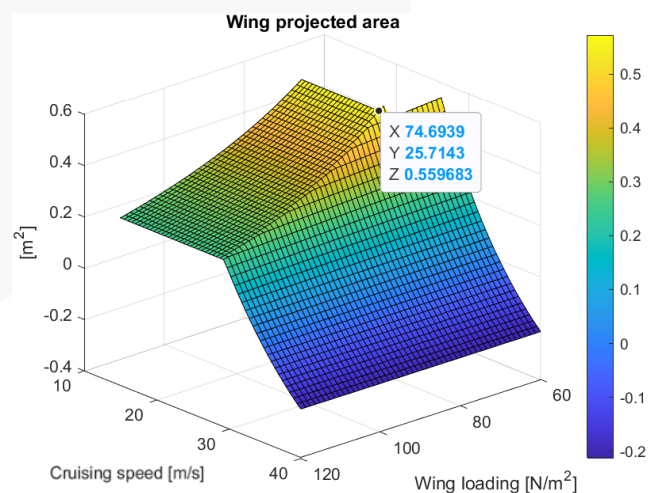


Figure 4. Wing area diagram.

The dimensions obtained by the code were used as a basis for the final dimensioning of the aircraft, working together with the performance area, the input variables were modified thus obtaining the predicted payload of 2.4 kg and wing area of 0.577 m².

Airfoil selection, positioning and testing

As for the airfoil selection, it was decided to divide the process into three phases:

1. Weighting of design parameters through QFD (Quality Function Deployment) methodology,
2. Grading of the geometric and aerodynamic criteria of the selected airfoils,
3. Carrying out the AHP (Analytical Hierarchy Process) to select the most adequate airfoil.

The implementation of the QFD helped to assign a relative weight for each of the design parameters according to ACC 2022's scoring system (see table 5).

Criteria	Importance [pts]		Cruise Lift Coefficient	Max Lift Coefficient	Min Drag Coefficient	Manufacturing Ease
Altitude after 60s	333	22%	3	9	9	1
Distance after 120s	333	22%	3	1	9	1
Payload [1000 pts.]	333	22%	9	9	9	1
Take-off bonus	130	9%	1	9	9	1
Wingtip load test	100	7%	1	1	1	1
Parts loss	100	7%	1	1	1	3
Manufacturability	200	13%	1	1	1	9
Total	1529	100%	3.61	5.16	6.91	2.18
Relative importance			20%	29%	39%	12%

Table 5. Evaluation of relative importance for the design parameters.

Next, the geometric criteria of the airfoils were evaluated, seeking mainly a thick leading edge, enough thickness to accommodate the main spar, and a thick trailing edge that prevents fractures when manufacturing. After that, the aerodynamic parameters of each profile were evaluated considering the following conditions for the analysis: a stall speed of 9.34 m/s, air density of 1.1536 kg/m³ and an operating range of 200,000-400,000 Re. Afterwards, the weighting for each profile was obtained (see table 6).

Airfoil	C _l Cruise Score	C _l Max Score	C _d Score
NACA 6412	8.12	8.85	9.26
GOE 227	10	10	7.86
NACA 7414	8.72	9.90	8.22
GOE 528	7.47	7.58	8.97
GOE 405	6.87	6.60	9.28
ST. CYR 24	6.89	7.20	6.94
SG6043	8.28	9.07	10

Table 6. Aerodynamical properties weighing.

Finally, the AHP methodology was applied, and a global grade was assigned to each airfoil (see table 7).

Airfoils								
Criteria	Importance	NACA 6412	GOE 227	NACA 7414	GOE 528	GOE 405	ST. CYR 24	SG6043
C _{d min}	39%	9.27	7.87	8.22	8.97	9.28	6.95	10.00
C _{l max}	29%	8.85	10.00	9.90	7.59	6.60	7.20	9.07
Manufacturing Ease	12%	10.00	7.50	10.00	8.33	6.67	8.33	5.00
C _l (Cruise)	20%	8.12	10.00	8.22	7.48	6.87	6.90	8.29
Total	100%	9.00	8.87	8.93	8.19	7.70	7.18	8.78

Table 7. Airfoil Analytical Hierarchy Process.

However, competition requirements led to the design of a cargo bay located inside the aircraft wing, which is why it was decided to look for an airfoil that would provide enough thickness in the central section of the geometry and thus, be able to save the load without issues. For this, we designed a pair of new airfoils through interpolation between NACA 6412, the AHP winner, and GOE 227, the thickest airfoil. Subsequently, an inverse design was applied to improve curvatures smoothness and to delay detachment, resulting in

BAGAFOIL 4 (14% thickness, located at the same place as the load) and BAGAFOIL 3 (the most efficient, located in the side section).



Figure 6. BAGAFOIL 4.



Figure 7. BAGAFOIL 3.

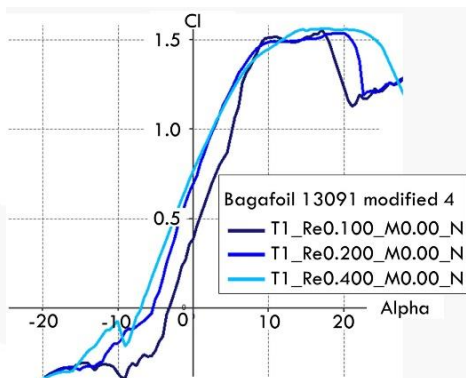


Figure 8. BAGAFOIL 4 C_l vs AoA graph.

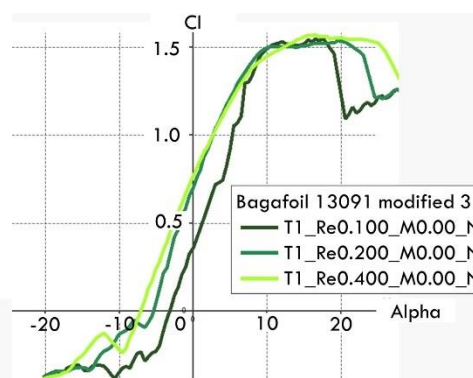


Figure 9. BAGAFOIL 3 C_l vs AoA graph.

Both airfoils present a behavior that prevents them from stalling immediately, maintaining a stable C_l in the range of 10° to 20° AoA, a behavior that favors wing performance. BAGAFOIL 4 reaches its C_{lmax} at 12.3° of AoA, BAGAFOIL 3 at 11.7° of AoA (see figures 8 and 9).

The aerodynamic efficiency of both airfoils corresponds to the Reynolds rate to which they are exposed according to their position in the wingspan. With BAGAFOIL 3 being the most efficient at low Reynolds is therefore the optimum to be used in the tip section (see figure 10).

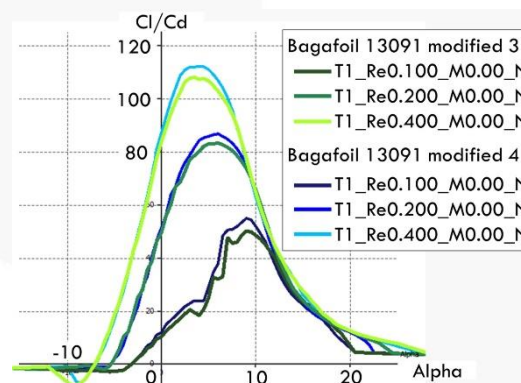


Figure 10. C_l/C_d vs AoA of BAGAFOIL 4 (green) and BAGAFOIL 3 (blue).

Geometry selection

Using geometric data obtained with MATLAB code and considering the drag reduction objective, it was considered the use of two wing planforms: Schuemann, because of the ease of manufacturing; and elliptical because of its ideal lift distribution. Consequently, a planform that combined both properties was selected (see figure 11). Then, a rectangular central section was added to save the payload, reducing the size of other surfaces that don't add any significant lift value, thus reducing drag.



Figure 11. Wing ultimate geometry.

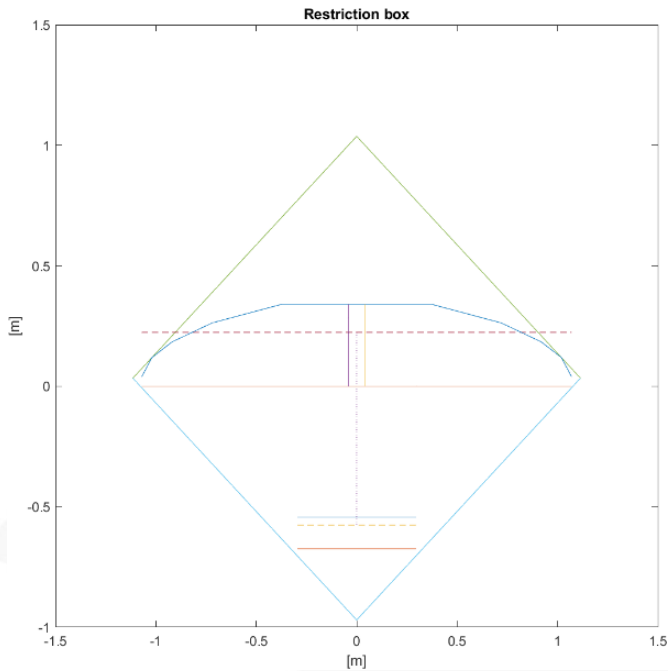


Figure 12. Arrangement of the aircraft within the restriction box.

From this geometry, the leading-edge curve behavior's formula was determined and introduced in a MATLAB code, which inserted it in the available space within the restriction box. By taking advantage of the constraint box's longest diagonal at a 98 degrees flexion and a distance between aerodynamic centers to the horizontal stabilizer of 0.80 meters, a maximum span of 2.17 meters was obtained (see figure 12).

Additionally, a dihedral angle of 11.5° was implemented, providing lateral stability improvement that helps restore its position after a crosswind. In addition to this, the configuration allows to accommodate the structural ribs to align with the main spar and a load can be carried within them.

Once the final geometry was configured, the geometric and aerodynamic properties were calculated and, making use of the Vortex Lattice Method analysis for

viscous flows, the aerodynamic properties were determined (see table 8).

Wing properties							
b	2.166 m	c_r	0.34	e	0.821	C_{Lmax}	1.43
S	0.577 m ²	c_t	0.04	C_{Lα}	4.432	C_{D0}	0.0158
AR	7.75	λ_{c/2}	12.09	C_{L0}	0.588	C_D	0.0214
TR	0.12	MAC	0.3 m				

Table 8. Wing geometric and aerodynamic properties.

High-lift device

For this competition, it was sought to implement the use of a high-lift device, in this case, it was decided to implement the use of flaps to help reduce the take-off distance and increase the maximum load of the aircraft, and for this, two options were evaluated: a simple flap and one slotted (see figure 13 and 14).

Both options were located at 80% of the chord and were analyzed in the ANSYS Fluent software to simulate the behavior of the flow in both devices and to obtain an approximation of the lift force generated by both with a maximum deflection of 25° .

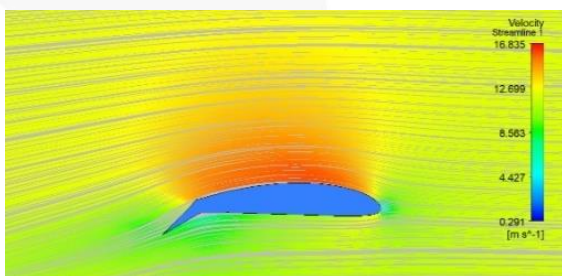


Figure 13. Flow analysis in ANSYS Fluent for simple flap.

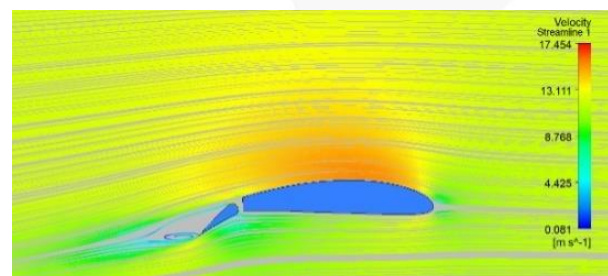


Figure 14. Flow analysis in ANSYS Fluent for slotted flap.

Finally, it can be observed how with the simple flap keep a higher speed difference compared to the slotted flap. It can also be noted that the simple flap maintains a cleaner flow on the trailing edge, unlike the slotted flap, where it can be seen how flow recirculation is created. For this reason, the simple flap offers a $C_L = 0.855$ and $C_L/C_D = 7.94$ compared with the slotted flap that offers a $C_L = 0.782$ and $C_L/C_D = 7.84$ combined with the ease of manufacturing, it was decided that a simple flap would be used.

CFD analysis

An analysis of fluids was performed in the ANSYS Fluent software to simulate the behavior of the flow over the wing with flaps retracted and one more over the wing with flaps extended (with a surface of 0.052 m^2), having as variables a temperature of 25°C , a pressure of 1 ATM, and a speed of 12m/s . The results obtained will be presented below.

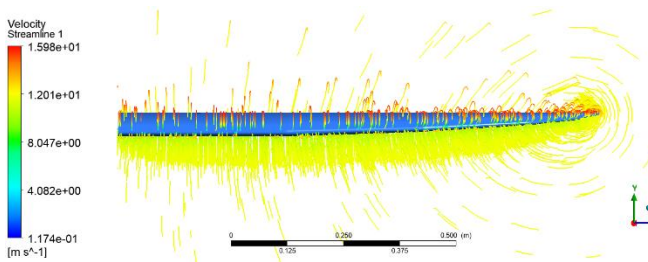


Figure 15. Analysis of wing without flaps in ANSYS Fluent.

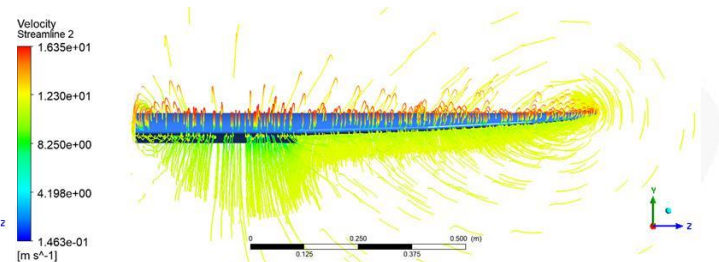


Figure 16. Analysis of wing with flaps in ANSYS Fluent.

For the final design, the flap was placed in the central section of the wing, considering that it is where the best lift is produced along the span and the geometry doesn't change, in the analysis of the wing with extended flaps it was possible to notice how the streamlines in the lower surface are deflated by the flap (see figure 16), which helps us with the increase of C_L , however, in this same image can be seen as the streamlines tend to deviate from the section where the flap ends, generating more vorticity in the wing and therefore increasing the total C_{D_i} .

The analysis helped us to measure the increase in the C_L of the aircraft thanks to the implementation of flaps in the wing design, since initially we reached a value of $C_L=0.296$ in the take off stage using the design shown in figure 15. With the implementation of flaps (figure 16), a value of $C_L=0.383$ was reached during the take-off stage.

With all this, we conclude that the dimension of our high-lift device meets the objective we are looking for, which is to increase the lift force by 29.39% compared with the wing without flaps and help us reduce the take-off distance, something that would be difficult to achieve without the use of this surface.

Lift Distribution

The method described in the book Theory of Wing Sections [3] was used to obtain the lift distribution graph, which provides a relationship between "basic distribution" (C_{l_b}), which depends on the geometric twist of the wing, and "additional distribution" (C_{l_a}), which varies with AoA . Because our wing has characteristics of an elliptical wing, it can be seen in the graph that it maintains a uniform distribution that avoids the pronounced drop of the C_L at the wingtips, therefore our design turns out to have good aerodynamic efficiency approaching the distribution line of an elliptical wing (see figure 17).

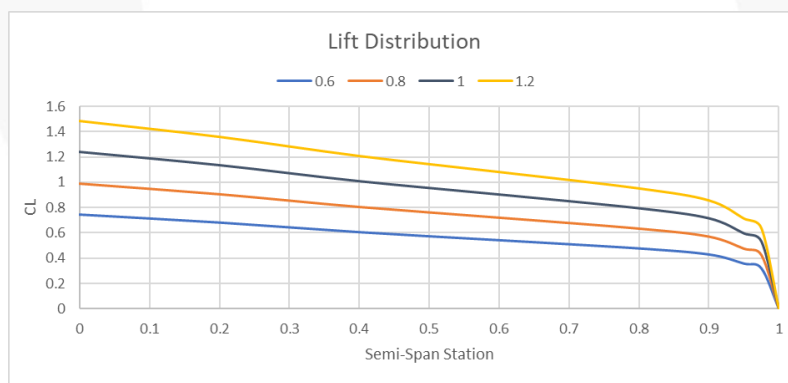


Figure 17. Lifting line along the semi-span.

Drag polar

To calculate the aircraft drag polar, a quadratic drag model described in the book General Aviation Aircraft Design [2] was drawn. For this, the aircraft was divided into its main components in relation to their drag contribution and subsequently the parasitic drag values were calculated for each one.

$$C_D = C_{D0} + k \cdot C_L^2$$

Equation 1. Simplified drag model.

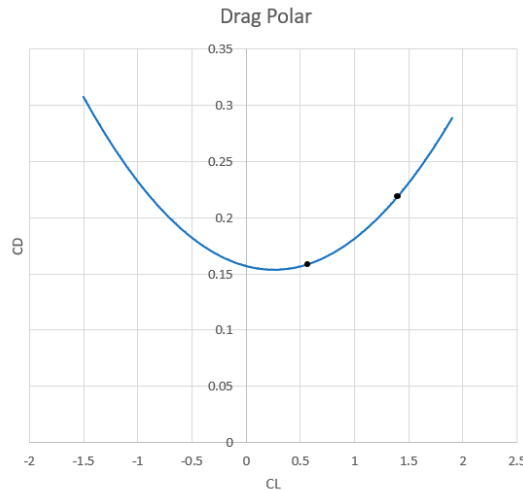


Figure 18. Drag Polar graph.

From the polar graph we can determine the drag of the aircraft at different configurations, considering the C_{L0} (0.588) we obtain a drag value of 0.159 and with the C_{Lmax} (1.43) a value of 0.222.

STABILITY AND CONTROL

Airfoil selection

Considering the density and viscosity of the air as static variables, as well as a cruising speed of 18 m/s and the aircraft's load capacity, an operational range of the vertical and horizontal fin stabilizers of between 10,000 and 1,000,000 Reynolds was established for the different analyzes that will be carried out. As seen in Figure 3, the amount of lift compared to the total drag and the different angles of attack experienced by the aircraft during flight show the efficiency of these airfoils at large Reynolds numbers, which is why they were chosen for meet the objective of this competition.

During the airfoil selection NACA 0012 was chosen for the vertical stabilizer and NACA 4412 inverted was chosen for the horizontal stabilizer. Both airfoils were chosen from an analysis in XFLR5, where the stability was found to be ideal for the final purpose of the aircraft and was supported by behavior data from pre-selected profiles, obtained in wind tunnel tests that are documented in the NACA-TR-824 report.

The NACA 4412 airfoil was chosen with the consideration that the maximum thickness had to be smaller than the wing's airfoil (13% - 14%). This airfoil meets the requirement of being 2% smaller in its maximum thickness than the wing's airfoils BAGAFoil 4 and 3. This also reduces the compressibility effects that the tail must endure, and since the lift coefficient of the horizontal stabilizer must be smaller than the wing's, the Mach number must also be smaller, according to the bibliography [4] [5] [6] [7]. It is vital that the NACA 4412 airfoil is inverted with its upper and lower surface opposite to the wing's airfoil's upper and lower surface respectively, as this generates the proper lift for the empennage.



Figure 19. NACA 0012.



Figure 20. NACA 4412 Inverted.

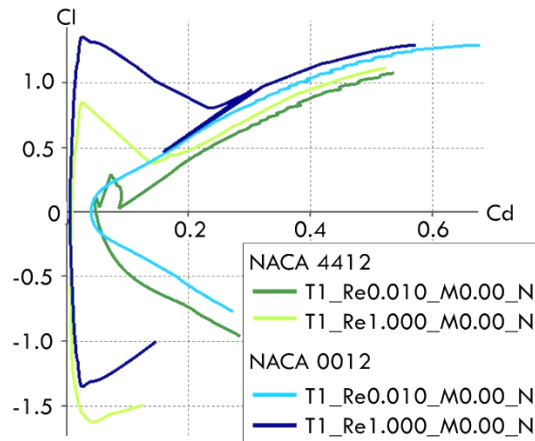


Figure 21. Analysis of the selected profiles for both stabilizers at 10, 000 & 1,000,000 Reynolds.

Tail sizing

To size both vertical and horizontal stabilizer areas, the following equations were used [1]. The volume coefficients were selected according to the requirements of the aircraft, considering the need for a small but adequate area, and considering the typical values for a "home-built" aircraft proposed by D. P. Raymer, thus selecting 0.4 and 0, 02 for the horizontal and vertical stabilizer, respectively.

$$S_{HT} = \frac{c_{HT}c_w S_w}{L_{HT}}$$

Equation 2. Horizontal surface sizing.

$$S_{VT} = \frac{c_{VT}b_w S_w}{L_{VT}}$$

Equation 3. Vertical surface sizing.

The distance between both aerodynamic centers (L_{HT} and L_{VT}) was established according to the angle that was given to the box for the assembled aircraft. It was done in such a manner so that the empennage would fit satisfactorily and prevent the stabilizers from exceeding the box's dimensions, whilst also providing adequate areas for the stabilizers, which is why the horizontal stabilizer was given a 0.8 m distance and the vertical stabilizer was positioned 0.822 m away from the wing's aerodynamic center.

Symbol	Value	Symbol	Value
C_{VT}	0.02	C_{HT}	0.4
S_w	0.577 m ²	S_w	0.577 m ²
b_w	2.14 m	C_w	0.3 m
L_{VT}	0.822 m	L_{HT}	0.80 m
S_{VT}	0.030 m ²	S_{HT}	0.0866 m ²

Table 9. Vertical (left) and horizontal (right) stabilizer dimensioning values for the different parameters.

Tables 9 show the remaining values for equations 2, which were obtained from the wing of our aircraft, which are the wing area (S_w), the mean aerodynamic chord (C_w) and span (b_w). Figure 22 shows the stabilizers' geometry (distance is measured in meters), considering that two vertical stabilizers will be used for the U-tail configuration.

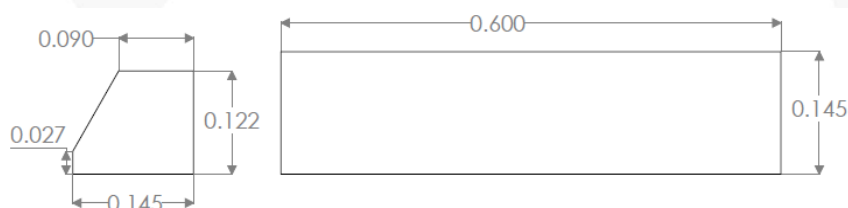


Figure 22. Vertical (left) and horizontal (right) stabilizer geometry.

Having an aspect ratio of 4.15 and 0.5 for the horizontal and vertical stabilizer respectively, the condition is to have an aspect ratio lower than that of the wing and with these values we obtain that.

Gravity center, neutral point, and static margin

$$X_{NP} = \frac{Cm_{\alpha}}{-CL_{\alpha}} + X_{cg}$$

Equation 4. Neutral point.

$$X_{CG} = \frac{\sum_{i=1}^n W_i X_{CGi}}{\sum_{i=1}^n W_i}$$

Equation 5. Center of gravity.

$$ME = \frac{X_{NP} - X_{CG}}{MAC} * 10$$

Equation 6. Static margin.

During the longitudinal static stability test of the aircraft, three stability conditions are considered: neutral, stable, and unstable. The proper location of the center of gravity with respect to the neutral point of the aircraft and the identification of the static margin are of vital importance when defining the proper load distribution across the longitudinal axis of the aircraft and when characterizing the behavior of the aircraft through one of the three previously mentioned stability conditions.

For the calculation of the neutral point, equation 3 was used considering the conditions of $Cm_{\alpha}=0$ and $C_{L_{\alpha}} = 0$ and the previous calculation of the center of gravity where the methodology of Mohammad H. Sadraey was used, which considers the mass of each of the components of the aircraft distributed along the longitudinal axis, the masses of the components are considered from table 1 and the equation that was used was the one proposed in the pre- report and is equation 4 [6].

The center of gravity was calculated at 0.103m from the leading edge of the wing. Considering this CG value, the neutral point was identified at 0.28 m. The stability and control area proposes a static margin for the aircraft of 6% since, according to Raymer's methodology [5], the recommendation is to have a range of 5% to 10% of static margin.

Identifying the neutral point, static margin, and MAC, we propose that the position of the center of gravity must be at 0.10m starting from the leading edge of the wing according to equation 4. With this position we ensure that the center of gravity will be ahead of the point neutral, which ensures that the empennage will have the ability to generate a negative moment coefficient with respect to the angle of attack to compensate for the positive moment coefficient of the wing and thus ensure that the aircraft will fly in stable conditions.

Longitudinal and lateral-directional static stability and control

The aircraft's equilibrium point is described in the Cm vs α graph, where the moment coefficient equals to 0 for a certain angle of attack. One of the requirements for the longitudinal static stability of the aircraft is that the slope of the curve must be negative, which can be verified through the derivative of the moment coefficient with respect to α . In this case, the analysis was made using the stability module of XFLR5. According to the results when $Cm=0$, the angle of attack will equal 2.058° , thus, this will be the optimum angle of operation for the aircraft. In the first graph (figure 23) the slope is negative, which means that it is stable.

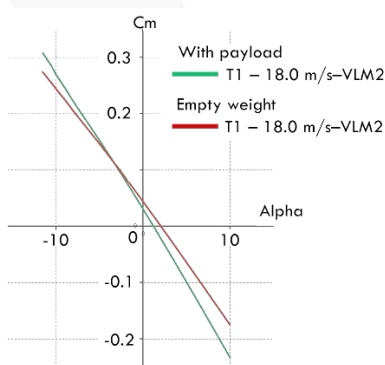


Figure 24. C_m vs α graph.

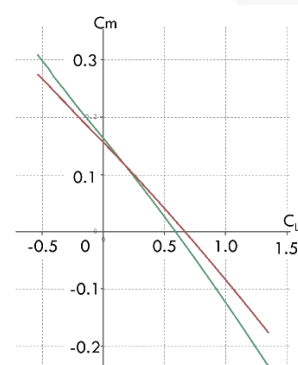


Figure 23. C_m vs C_l graph.

For the aircraft to take off, a positive lift coefficient is required in the equilibrium point to generate lift. This can be appreciated in the second graph (figure 24), where the curve intercepts the x axis (C_L) in a positive value. The figures 23 and 24 were obtained from the analysis performed by the XFRL5 software.

Dynamic stability

	Longitudinal modes				Lateral modes			
	With payload		Without payload		With payload		Without payload	
λ_1	-8.29+	-12.05i	-7.49-	-9.87i	-16.3+	0i	-14.2102+	0i
λ_2	-8.29+	12.05i	-7.49+	9.87i	-0.6162+	-3.87i	-0.6117-	-3.41i
λ_3	-0.02123+	-0.8125i	-0.0169-	-0.8969i	-0.6162+	3.87i	-0.6117+	3.41i
λ_4	-0.02123+	0.8125i	-0.0169+	0.8969i	0.1318+	0i	0.1497+	0i

Table 10. Longitudinal and Lateral eigenvalues according to XFRL5.

For longitudinal motion, both λ_1 and λ_2 real parts of the Short Period mode eigenvalues are negative, thus, it can be predicted that the plane is stable in a Short Period mode (see figure 25a). Also, the loaded plane has a damping ratio of 0.566, and a 0.604 ratio for the empty calculation, indicating that the aircraft can bring itself back to a stable longitudinal position (see figure 25). Furthermore, λ_3 and λ_4 eigenvalues are negative, which implies that the plane is stable in a Phugoid mode. The mode presents a positive damping ratio of 0.026 and 0.018, meaning that the aircraft may encounter some issues damping out (especially when loaded), but it's able to bring itself back to a stable longitudinal position (see figure 25b).

Besides, for lateral motion, the eigenvalue λ_1 corresponds to a highly convergent, damped, and stable roll mode with a negative eigenvalue (see figure 25c). Also, both λ_2 and λ_3 are associated to the Dutch-roll mode of the plane, and the plane real negative parts of its Dutch-roll mode eigenvalues indicates that it is stable (see figure 25d). λ_4 eigenvalue represents the spiral mode which can be either convergent or divergent. A negative eigenvalue indicates spiral stability, thus, because of our value corresponds to a positive one, we can conclude that the plane is unstable for a spiral mode. The issue has been treated to redistribute dimensions and weight, but the actual configuration still is the most stable.

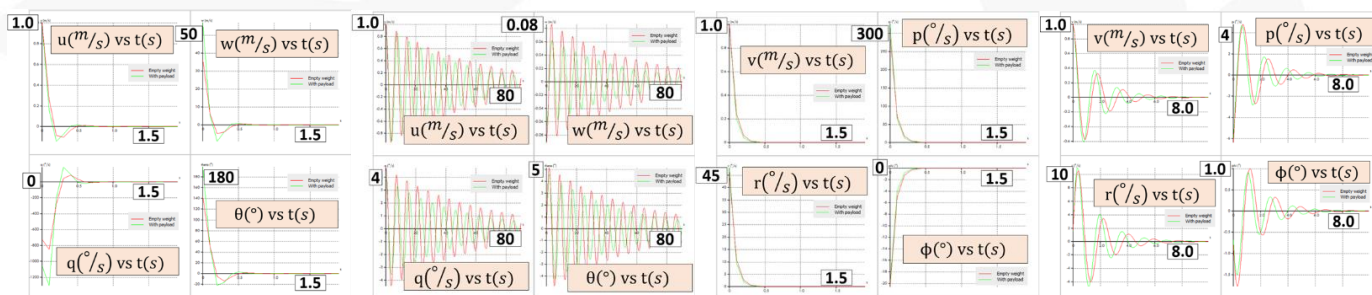


Figure 25. (From left to right; red line for loaded; blue line for empty) a) Time response for short period mode loaded and empty; b) Time response for phugoid mode loaded and empty; c) Time response for roll mode loaded and empty; d) Time response for Dutch-roll mode loaded and empty.

Control surfaces

Aileron sizing

For this project, it was decided that the optimal dimensions for the ailerons, considering the deflection angles and structural limitations, should be a length of 0.34 m (32% $b_w/2$) and a width of 0.075 m (25 % C_w) located at 0.68 m from the airplane's longitudinal axis. Those proportions were chosen considering Sadraey's recommendations for length (40-80%) and width (15-25%) and the length constraints that the loading bays create [8].

To validate the proposed dimensions for the aileron, the method of the aileron roll response was used [9].

The obtained values the roll control parameters prove a satisfactory roll control authority and response time over the aircraft due to aileron deflection considering the maximum payload, since we have a fast response time of 4s and 3.2s and that the roll control values are within the range of 15°/s and 30°/s, which are recommended values for this type of aircraft according to Sadraey's.

Roll control parameters	Take off speed	Cruise speed
$C_{l\delta\alpha}$	0.001185	0.001672
C_{lp}	-0.01561	-0.01551
P	12.8 °/s	27.2 °/s
Steady response time due to aileron deflection	4 s	3.2 s

Table 11. Values for roll control parameters.

Elevator sizing

The dimensions of the elevator according to Sadraey's it is recommended that the length should cover 80-100% of the length and width 20-40% of the horizontal stabilizer, 0.56 m long (83% b_H) and 0.057 m (40% c_H) wide. To determine if the elevator can satisfy the pitch, take-off and landing requirements, the angle of attack effectiveness of the elevator (τ_e) must be calculated. To achieve this, the resultant value of equation 6 must be smaller than 1°.

$$\tau_e = \frac{C_{L_h} - \alpha_h}{C_{L_{\alpha_h}} \delta_E}$$

Equation 7. Angle of attack effectiveness of the elevator.

Symbol	Value
C_{L_h}	0.624
$C_{L_{\alpha_h}}$	0.0651
α_h	2.058°
δ_E	20°
τ_e	0.37°

Table 12. Values for equation 6.

Table 12 shows the values used for the calculation of the angle of attack effectiveness and the obtained result is 0.37°. The elevator will satisfactorily meet the rotation, takeoff, and landing requirements because we have an effective angle of attack of less than 1°. Consequently, the tail will successfully accomplish the requirements.

Rudder sizing

The dimensions of the rudder according to Sadraey's it is recommended that the length should cover 70-100% of the length and width 15-40% of the vertical stabilizer, 0.095 m long (77% b_V) and 0.055 m (37% c_V) wide. To determine whether these sizes were adequate to satisfy the directional control/compensation requirements, the rudder angle of attack effectiveness was calculated using equation 8 and had to be less than 1° to accomplish the objective.

$$\tau_r = - \frac{C_{n\delta R}}{C_{L_{\alpha_V}} \bar{V}_V \eta_V \frac{b_R}{b_V}}$$

Equation 8. Rudder angle of attack effectiveness.

Symbol	Value
$C_{n\delta R}$	0.00114
$C_{L_{\alpha_V}}$	0.002038
\bar{V}_V	0.02
η_V	91.76
b_R	0.095m
b_V	0.122m
τ_r	0.39°

Table 13. Values for equation 7.

The rudder angle of attack effectiveness was equal to 0.39°, thus, the rudder will be able to satisfy the most critical requirement which is the directional control/compensation with the combination of vertical tail and center of gravity of the aircraft.

STRUCTURAL DESIGN

The aircraft's components are designed under certain requirements to fulfill the flight mission with the best performance possible. There are two types of loads that the aircrafts have to endure: *In-flight loads* which

are due to symmetrical and asymmetrical flight, or atmospheric gusts from any direction, and *on-ground loads* that result from ground handling and field performance (e.g. in static, takeoff and landing) [10].

The topics addressed in this section are payload placement, fuselage design, landing gear design and design and analysis of the main structural components. The structural analysis will be limited to static analysis and will focus on in-flight loads, specifically during cruise flight in which the load factor equals 1. Besides, to guarantee the aircraft's structural integrity in any flight phase an ultimate load factor of 2.7 will be used. To calculate the ultimate load factor's value the methodology and approximations on Sadraey's book [8] were used, along with equation 9 considering a $n_{max} = 1.8$:

$$n_{ult} = 1.5n_{max}$$

Equation 9. Ultimate load factor.

Payload placement

The aircraft was designed with the payload bay located on the central part of the aircraft and is comprised of two main payload bay spaces. To take advantage of the volume given by the natural design of the airplane, the first payload bay was positioned within the wing's structure, in which six 300g blood bags will be carried. To complete the additional cargo, a second payload bay was designed and positioned within the fuselage, it does not have a structural purpose other than hold the payload and it has an aerodynamic shape to diminish drag. The placement of both payload bays was determined considering how they will affect the CG, that is the reason why the first bay is divided symmetrically within the wing and the second bay is placed slightly in front of the desired CG, to compensate the tail's weight.

Fuselage

The fuselage is positioned under the wing, and it oversees keeping together all the airplane's parts like the empennage, wing, landing gear and motor. As the figure 26 shown, the aircraft has a carbon fiber square tube with a total length of 1.17m that starts in the motor and finishes in the empennage and all the devices are hold there. For this competition the fuselage was aerodynamically designed to reduce the drag.

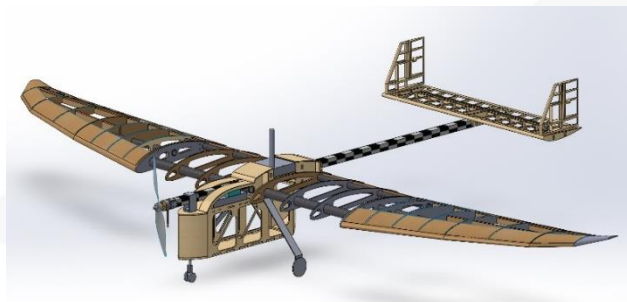


Figure 26. Aircraft model.

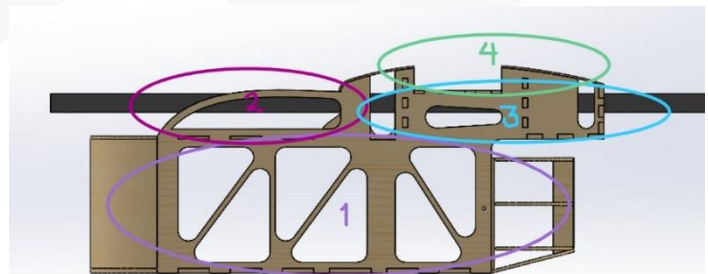


Figure 27. Fuselage main sections: 1- payload bay; 2- electronics bay; 3- Wing Subsection; 4- Measurement box coupling.

The fuselage was designed considering a high-wing aircraft design. It counts with 4 main sections, as shown in the figure 27: the payload bay, the electronics bay, the wing subsection, and the measurement box coupling. The payload bay and the wing subsection are made of pine wood to provide structural rigidity. The electronics bay is a balsa wood component provided with an aerodynamic form to reduce the total drag of the fuselage. Both the payload and the wing subsection have special features: the payload bay is coated with PEVA to prevent any tears in the blood bags due to the friction they would have with the wood; meanwhile, the wing subsection its designed as an aerodynamic profile (sideview) to allow an organic attachment between the fuselage and the wing. Finally, it was decided to ubicare the measurement box coupling as close as possible to the CG of the aircraft, since this positioning provides the smallest G-Forces and the smallest bank angles. Moreover, the top of the fuselage was selected to place this component because this way an unobstructed view of the sky and an easy assembly and disassembly are provided.

Stress analysis

To validate the design a structural analysis of the main components was carried out. Given that there will be a static load test during the competition, it was necessary to determine whereas these components will be able to withstand the weight of the aircraft itself and the payload. For this reason, it was decided to make a stress analysis in the critical components: main beam, wing, and landing gear.

Main beam

The stress analysis for the main beam required the use of the ultimate load factor and the resultant loads produced by each main element of the aircraft. The result of this study led to the shear stress and bending moment diagrams in the next figures.

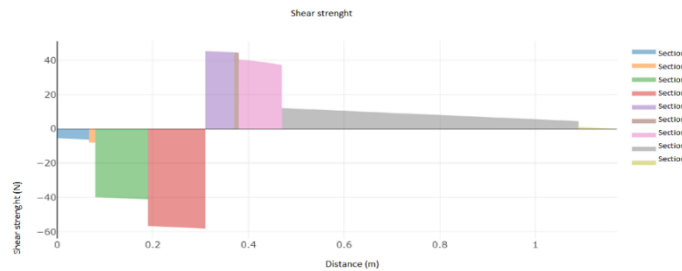


Figure 28. Shear stress diagram.

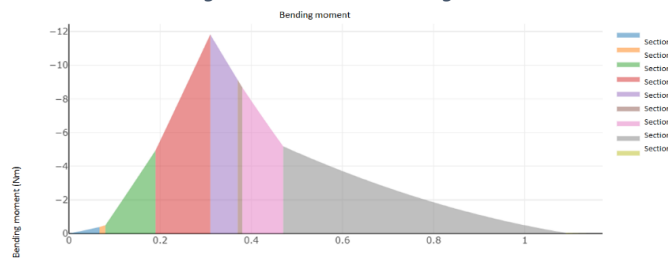


Figure 29. Bending moment diagram.

As it can be seen, the maximum shear stress and the bending moment happen at a distance of 0.31m, approximately at the center of gravity, which makes sense as only the components' weights were considered for this analysis. Therefore, to determine if the beam would be able to tolerate the loads the equation 9 was applied with a maximum bending moment of 11.8Nm, the distance from the centroid to the cross-section surface and its moment of inertia.

$$\sigma_{max} = \frac{Mc}{I}$$

Equation 10. Maximum bending stress.

In consequence a maximum stress of 13.47MPa was obtained, which is less than the Ultimate Tensile Strength (UTS) of 4.59GPa that many manufacturers provide for similar profile. It can be concluded that the main beam will be very likely to bear all the loads without failing.

Wing

The wing is divided in three parts to ease the transportation. As it was mentioned before, a payload bay is contained in the wing. To guarantee the structural integrity of the central section of the wing containing the bays, it was decided to manufacture the upper and lower surface in carbon fiber and have the main and support spars crossing through them. Meanwhile, the other sections' (wingtips) frameworks are made of pine wood and cotted with Monokote.

For this analysis it was proposed to idealize the wing as a cantilever beam supported at the fuselage and to use the main spar's cross section to define the cross section of the cantilever beam.

However, the design of the wing structure doesn't contemplate a spar that could be define as the main spar.

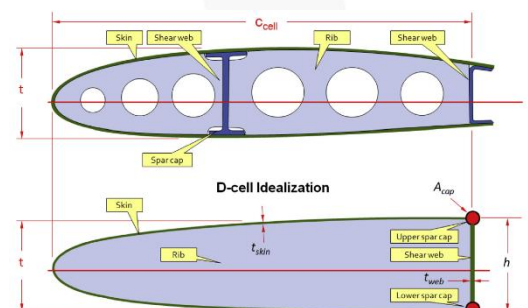


Figure 30. Idealization of the wing's structure.

Due to this difficulty, it was decided to use the assumptions described by Gudmundsson [2] an idealize the wing structure as a D-cell section and a main spar, as shown in figure 30. The resulting idealized main spar is shown in figure 31.

In the analysis the three primary loads that will act on the aircraft wing will be evaluated: Aerodynamic lift, load due to the structural weight, and load due to the weight of the blood bags contained in the wing's payload bay. These loads are perpendicular to the wing surface, and the magnitude of the first two loads varies along the length of the wing.

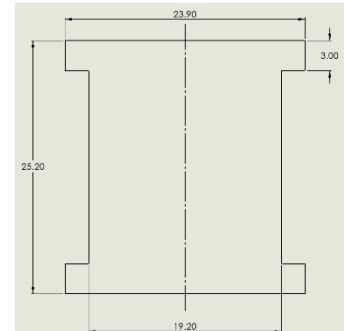


Figure 31. Idealized cross section.

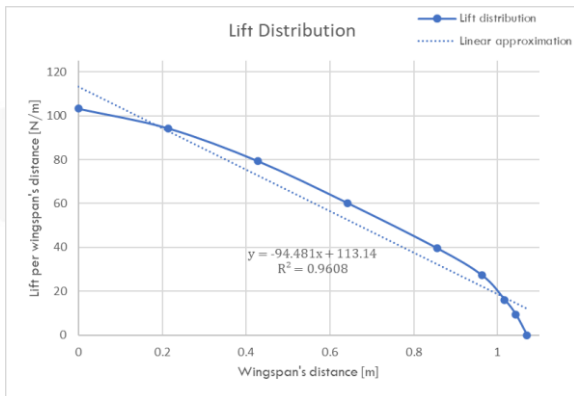


Figure 32. Lift distribution graph.

The aerodynamic lift was described by the lift distribution's graph shown in figure 32. The lift coefficient $C_l = 1.44$ was used to create this graph since it is the critical coefficient for the airfoil. A linear approximation was calculated to be used in the MEF software and is also shown in the same picture.

The aircraft's load factor can be calculated integrating the distributed load and multiplying by 2 using equation

11. Considering that $W_{to} = 51.993 N$, the load factor is 2.7. As the critical C_l was used, this load factor can be considered n_{ult} , which justifies this values calculation at the beginning of this section.

$$n = \frac{Lift}{W_{T0}}$$

Equation 11. Load factor.

To calculate the weight distribution on the wing structure the method described by Doherty [11] was used. Two different functions were proposed to calculate the wing's structure, since the wing has two different materials, considering each section length and an approximate mass of 200g for the carbon fiber central section and 150g for the wing tips built with balsa wood covered with Monokote. The load distribution of the weight on the wing structure, as well as the functions used on MEF software are shown in figure 33. To determine the load, withhold by the cargo bay, the weight of each blood bag was idealized to 300g as a punctual load located at the CG. The stresses and strains analysis were performed in the software FEM ANSYS APDL. Since the idealized beam resulted from the use of spars of different materials (wood and carbon fiber) the simulation was performed considering only pine wood given that is the material with worse mechanical properties and this analysis would generate critical conditions for the beam. Figure 34 shows the total deflection of the wing, where the maximum is 18.7mm on the wingtip. On the other hand, the shear stress and bending moment to the beam are $-54.99 N$ and $22.76 N \cdot m$ respectively.

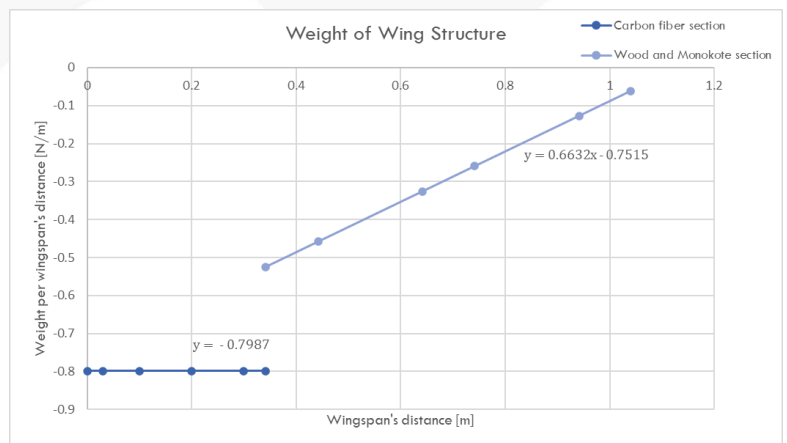


Figure 33. Weight of Wing Structure.

With the previous data it can be determined if the circular spar with smaller cross section would withstand the load applied on the wing. It was assumed that the spars would take half of the reactions, this is $S = -27.495 \text{ N}$ y $M = 11.38 \text{ N} \cdot \text{m}$. In figure 35 shows that Von-Mises maximum efforts on the spars are 64.6 MPa , which are much less than the Ultimate Tensile Strength of 4.89 GPa that many manufacturers provide for similar profiles.

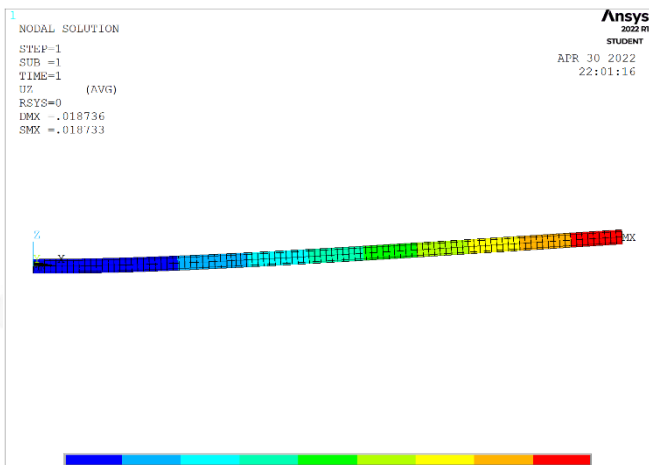


Figure 34. Total deflection of the wing [m].



Figure 35. Von-Mises stress in a carbon fiber spar [Pa].

Landing gear

A tricycle configuration was selected for the landing gear for its stability at landing. It is fixed to the main beam and in contact with the wing's beam, in this way, it will be in contact with more components to distribute the energy and thus, reducing the impact.

Considering the surface of the runway the wheels selected are wide, large and light to avoid that grass entanglement could stop the aircraft. Besides wide wheels distribute the pressures of the aircraft on the land preventing it from getting buried.

The landing gear was analyzed to ensure that it will withstand the forces on the landing stage. A static analysis was performed on the software ANSYS. To probe that it will endure as in a dynamic analysis the maximum loads during landing were employed to ensure this test.

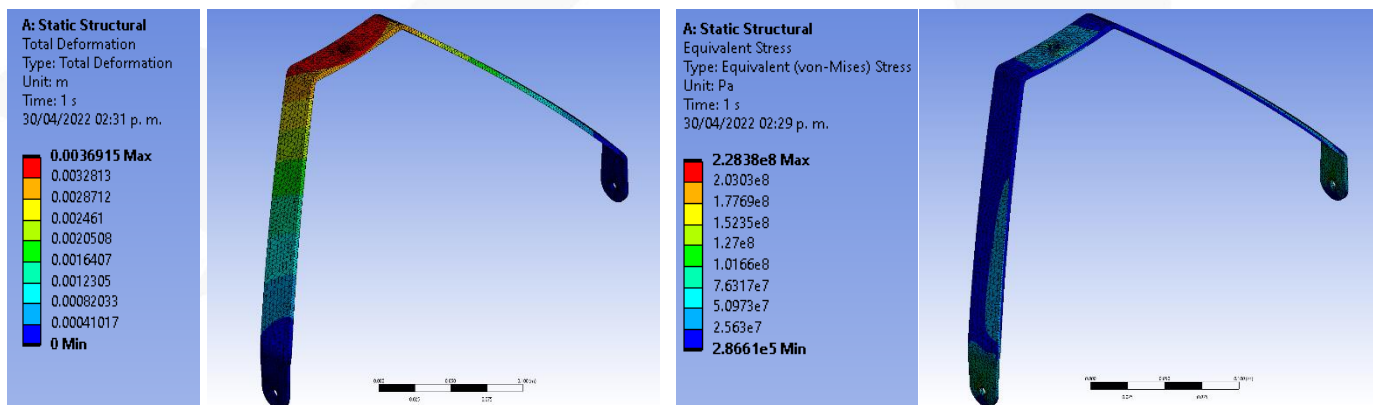


Figure 36. Total deformation analysis (left) and equivalent stress analysis (right), with their respective scales.

For the landing gear analysis, the loads were placed on the lower part in direction with the X axis as shown in figure 36. This is the place where the wheels are placed, which are the components that will transmit the energy from the impact to the rest of the aircraft. For this analysis the ultimate load factor was used to submit the component to the highest stress possible. This results on a Von-Mises effort of 228 MPa , which is less than the 415 MPa yield strength of the material. With this we can conclude that the aluminum plate used to manufacture the main landing gear resists the impact. In addition, the analysis shows that there will

be a maximum deflection of 3.6mm at landing, which is not critical. All this ensures the integrity of the main landing gear for the competition.

PERFORMANCE AND ELECTRICAL PROJECT

The Performance area makes the analysis of the aircraft behavior through different stages, evaluates the propulsion combinations and studies the electronics components that are required to achieve the aircraft’s mission. For this competition, taking-off in less than 40m with the most possible payload, ascending to the highest altitude allowed and traveling a corresponding distance are reviewed in the next sections.

Propulsion model

The first task was choosing between a puller and a pusher configuration as some UAV that transport medical supplies use the latter, although it is still not as common as the former. After some research (as the team has never used a pusher rotor), the puller configuration was selected as the pusher presented various disadvantages that include reduction in the performance during take-off, less efficiency as the flow becomes turbulent, possibility of difficult motor cooling, and others [12].

After this, the two main elements were analyzed to obtain the speed-thrust relation, which was required for the early wing dimensioning. As the motor is a fixed choice, the focus was set on the two propeller options, so they were both compared under the following parameters:

1. Software approach: using Ecalc to analyze the whole propulsion system with each propeller, the greatest static thrust was obtained with APC model (although the difference was just 6 grams).
2. Data availability: the data chart of the APC model was easily found, whereas not much was discovered about the Aeronaut Cam Carbon one.
3. Product acquisition: APC models are easier to acquire because of the teams’ location.

Therefore, the APC 10x6E was chosen. With both motor and propeller, the speed-thrust relation was calculated through different methods to comprehend the nominal behavior of the system: the APC data chart using the 9000RPM values as seen in the Ecalc preliminary test, its density adjustment, and the software Motocalc. The former presented the most consistent and exact values, which led to the required equation of the propulsion model and the graph in figure 35 and 36.

$$T(V) = (-0.010229V^2 - 0.10437V + 12.649) \frac{\rho}{\rho_0}$$

Equation 12. Airspeed vs. Thrust equation.

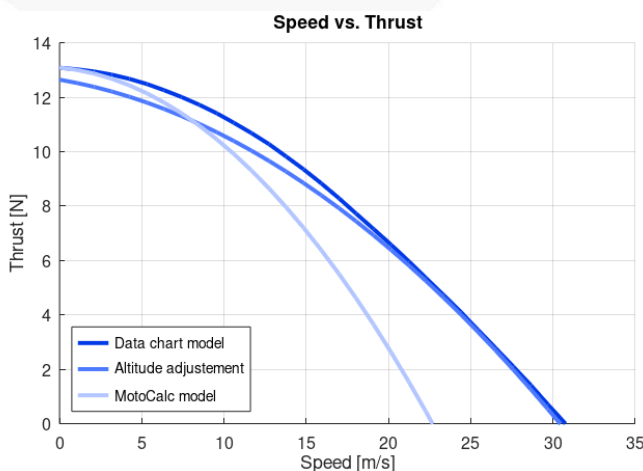


Figure 27. Speed vs thrust graph of the propulsion.

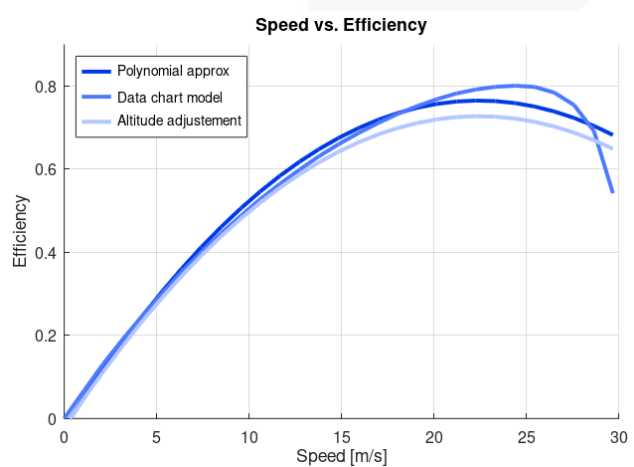


Figure 26. Propeller speed-efficiency graph.

Additionally, the APC data was used to obtain the propeller efficiency, required in the ROC study.

Available vs. Required Power and Thrust

The graphs of figure 38 represent the limits of the power and thrust of the propulsion system. The available thrust is obtained through the equation above, while the required is calculated equalizing the thrust to the drag. It can be observed that in the range of speed that the aircraft works, the required thrust is lower than the available thrust. On the other hand, the power available is also obtained through the propeller data chart, and the required with the values of the drag and lift coefficient as explained in Rodrigues' book [11]. And as in the case of the thrust, the power required is lower than the available power of the engine.

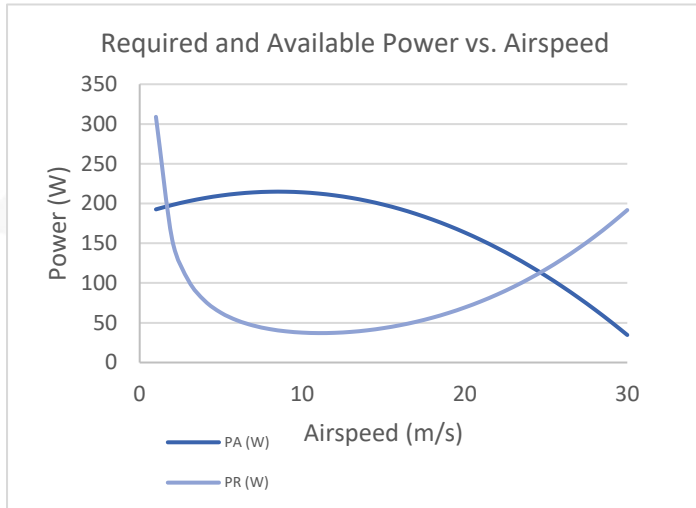


Figure 30. Required and Available Power vs. Airspeed.

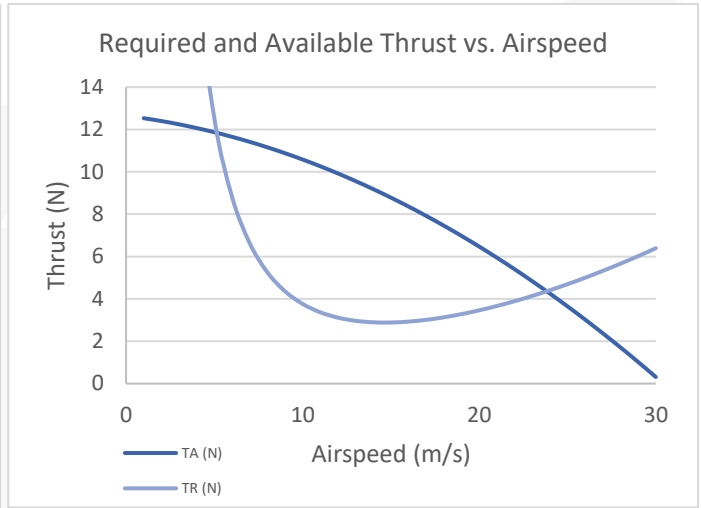


Figure 29. Required and Available Thrust vs. Airspeed.

Take-off total mass and take-off distance

To know the maximum mass that the aircraft can lift, the calculation was made to know the value if the aircraft would take-off in 60m and 40m. The methodology shown in another of Sadraey's books [12] was applied to estimate the different cases in which Zotz has flaps on and off for this stage.

$$S_G = \int_0^{V_{To}} \frac{mV}{T - \mu N - D} dV$$

Equation 13. Take-off distance without flaps

$$S_G = \int_0^{V_{To}} \frac{mV}{T - \mu mg - (1/2)\rho V^2 S (C_{D_{To}} - \mu C_{L_{To}})} dV$$

Equation 14. Take-off distance with flaps.

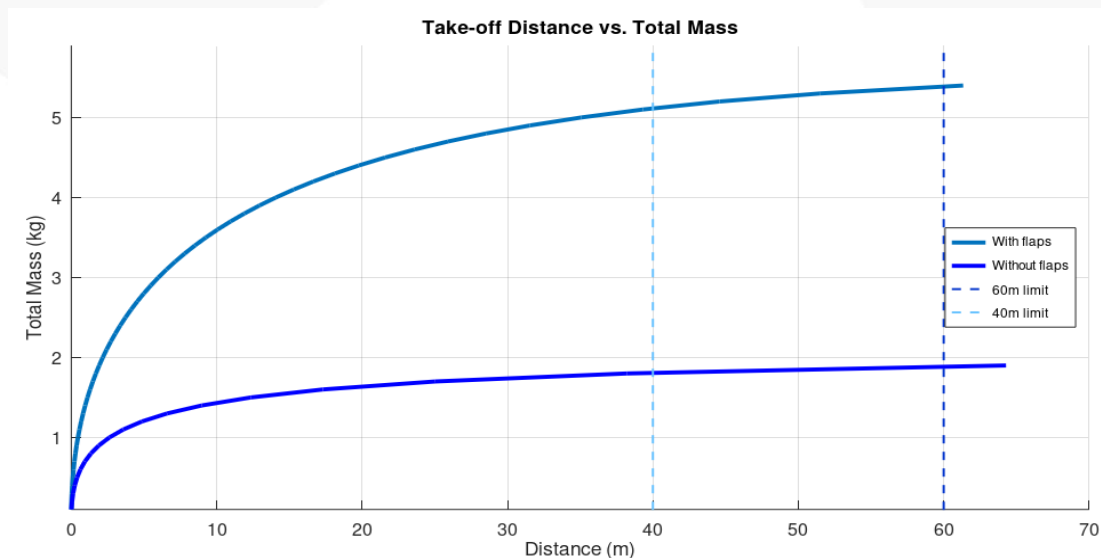


Figure 31. Comparison between the required distance for taking-off with and without flaps.

With flaps, a maximum total mass required to take-off at 60m would be around 5.4kg, and at 40m would be 5.1kg. whereas the case without flaps illustrates that the mass must be very low to take-off in the required distance.

Rate-Of-Climb

Because of one the requirements ask to ascend 100m in a period of 60s, the ROC analysis was applied as it states the aircraft's vertical speed and an altitude variation with respect to a period. Using equations 13, the diagram in figure 40 was obtained.

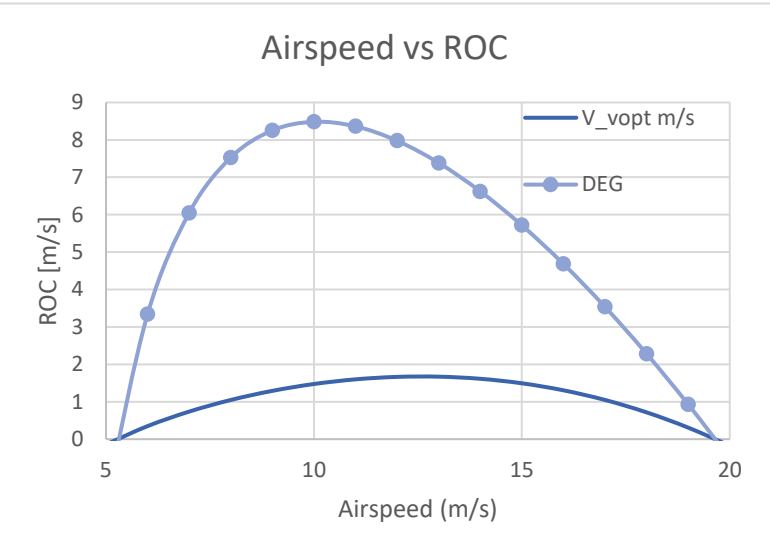


Figure 32. ROC and climb angle.

$$ROC = \frac{TV - DV}{W}$$

Equation 15. ROC speed

$$\sin \gamma = \frac{T}{W} - \frac{1}{L/D}$$

Equation 16. Climb angle

The optimum values are a speed of 1.6m/s and a climb angle of 8.36°. On account of these results, an approximation of altitude can be calculated using the climb time, which, although settled on 60s, was considered as 50s because the flight time begins when the aircraft reaches a speed of 5 km/h (measured by the logger), and as the take-off speed is greater than it, the climb time will begin running before the aircraft leaves the ground. Therefore, it is estimated that Zotz will reach an 80m height.

Turning Rate

The turning rate is a mathematical function when the airspeed and the bank angle are related and, in this way, get the distance that the aircraft needs to make a turn. Following Gudmundsson's method [2] with equations 17 and 18, the turning rate obtained is 11.4815m. With these results, the bank angle can be acquired solving it from the equation 4. Based on this a bank angle of 20.013° was acquired, which is lower than the maximum angle allowed of 40° in order not to lose the GPS signal.

$$R_{turn_{min}} = \frac{V_{Rmin}^2}{g \sqrt{n_{Rmin}^2 - 1}}$$

Equation 17. Minimum turning rate equation.

$$\phi = \tan^{-1}\left(\frac{v^2}{gR}\right)$$

Equation 18. Bank angle equation.

Flight Time and Range

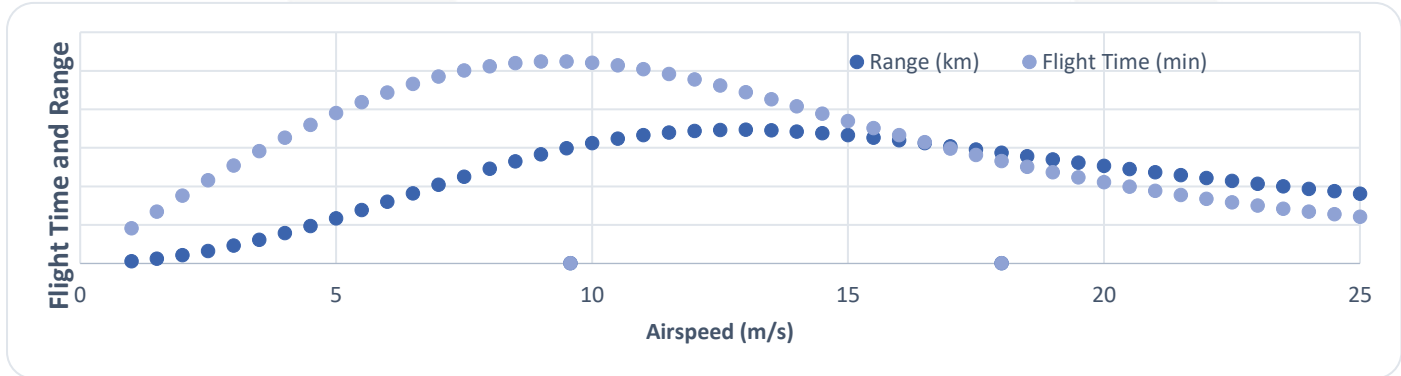


Figure 33. Flight time and range.

After the numerical calculations that were made with the battery, the engine, power and efficiency, the estimated flight time and range were obtained based on airspeed and the graph of figure 41 was obtained. Based on this figure the airspeed chosen for the analyses is the cruising speed which is 18m/s. With this airspeed the flight time is 2.9 min, and the range is 2.194km.

Flight envelope

The load factors that constrain the aircraft performance are portrayed on the flight envelope. Equally, the following plot provides speed limitations as well as maneuvering speed which are essential for a pilot.

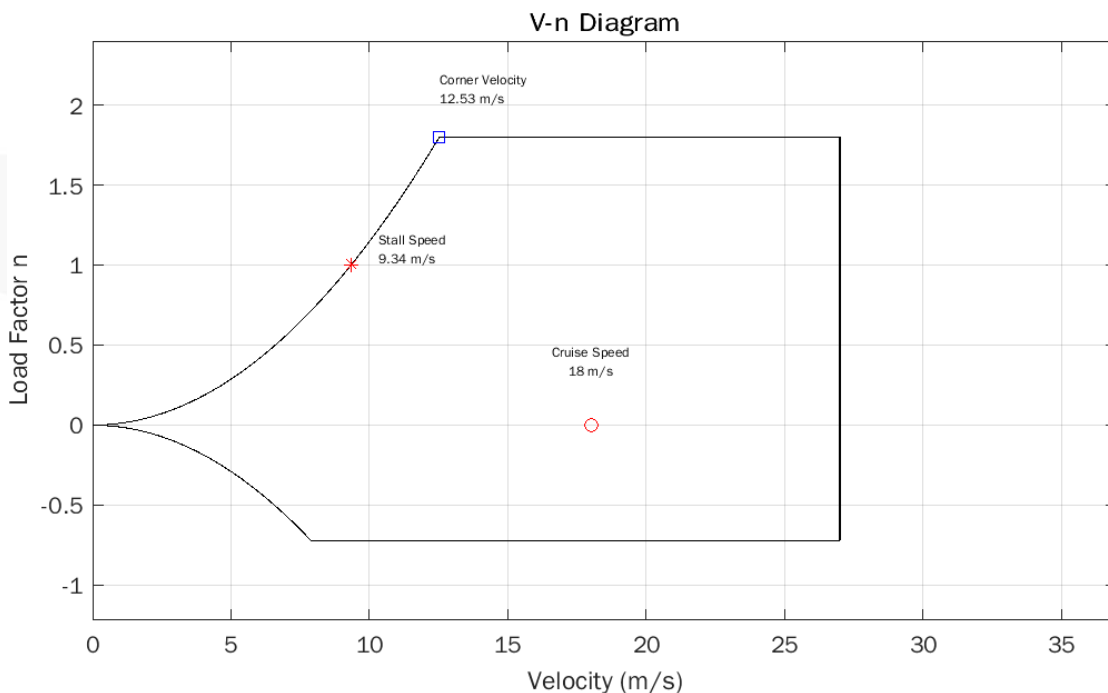


Figure 34. Flight envelope diagram.

Servomotors

To define the required torque for the control surfaces, the following formula was used:

$$torque = 8.5 \times 10^{-6} \left(\frac{C^2 V^2 L \sin(ah) \tan(ah)}{\tan(as)} \right)$$

Equation 19. Required torque for aircraft surfaces.

According to the data provided by stability and control area, the following table was made.

Surface	Required Torque (kg-cm)	Chosen Servo	Actual Torque (kg-cm)
Rudder	0.1592	SH-0350	2.6
Elevator	1.3158	SH-1350	4.6
Aileron	0.5819	SH-0254	3.9
Flap	2.6218	SH-1350	4.6

Table 14. Required servomotors for each surface.

For the surfaces, the chosen servos were Savox; the main reason was the relation weight-torque, as the aircraft must be light and the servos cannot be too heavy, but they must be able to move the surfaces, and these options accomplish these requirements with a high security factor. For the Nose Gear the selected servo is a Savox SH-1350, calculated using the conventional torque formula with a 15% of the total mass of the aircraft [8] and the displacement of the nose gear. These are also motors that the team has in existence and therefore can already use and test.

Batteries selection

For this component, the minimum parameters that the battery must fulfill are defined by the flight task, starting with the minimum flying time settled on 240s, the motor current defined by its datasheet and a security factor of 1.5. With this information, the equations 20 and 21 can be applied [6].

$$q_{bp} = n_{bp} \cdot t_{min} \cdot I_{max}$$

Equation 20. Minimum battery capacity in mAh.

$$C_{rating, bp} = \frac{I_{max}}{q_{bp}}$$

Equation 21. Minimum battery C-rating.

As a result, a 3s LiPo battery of at least 3000mAh and 15C is required. This combination can lead to a discharge of up to 45A if needed, accomplishing the 30A requirement. This also establishes an ESC of the same amperage at least. Contrary, the secondary battery was decided to be a 2s LiFe or LiPo battery of around 700mAh considering the experience of the team's last competition as inspections with 7 servomotors made a battery of the same characteristics to last more than 30 minutes in statics tests and with 5 bigger servomotors and an ESC lasted for two to three flight patterns.

However, the brand and model for the batteries cannot be described by now as its transport is a complicated task to satisfy from Mexico; therefore, they are going to be held to availability in Germany and the research is on the way to buy them there.

Aircraft's electrical model

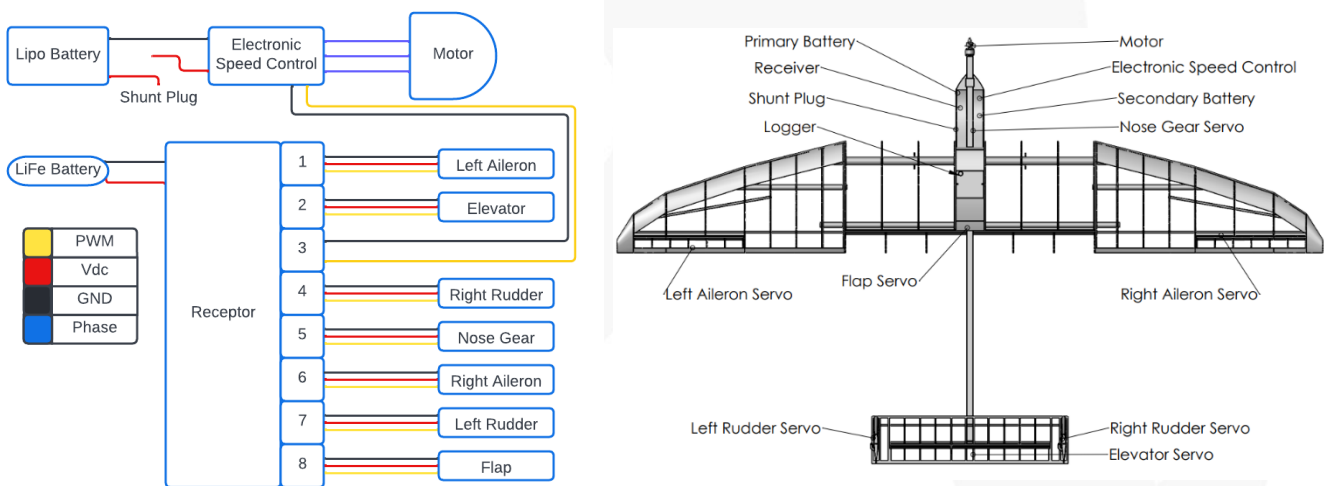


Figure 35. Electrical model (left) and component's locations diagram (right).

The left diagram of figure 43 shows how the aircraft propulsion and actuators systems are connected and powered separately, including the channels where each servo and the ESC are plugged in (without using a BEC). The picture on the right illustrates each of the electronics components' locations in the aircraft, including the logger, which is positioned above the PTR and a certain distance from the receiver so that it can avoid losing the signal.

PAYLOAD PREDICTION

The net mass (load) m_L carryable by the aircraft is given by the equation 22.

$$m_L + m_a = \frac{C_L V^2 S}{2 F_s g} \rho$$

Equation 22. Mass solving from the lift equation.

In order to consider a density-dependent function of mass, the next values are substituted in the previous equation: C_L of 0.5442, V of $18 \frac{m}{s}$, S of $0.577 m^2$, F_s of 1.28, g of $9.81 \frac{m}{s^2}$, m_a of 2.3 kg. However, the load prediction is required to be a function of the altitude. Therefore, the next ISA expression is used to obtain a density-altitude relation.

$$\rho = \rho_0 \left(\frac{T_0 + \lambda z}{T_0} \right)^{\frac{g}{R\lambda} - 1}$$

Equation 23. Density-altitude ratio.

Subsequently, a MATLAB script is developed with the purpose of computing the slope-intercept equation and its plot shown below. The result at Munich's altitude states that a 2.42kg payload can be lifted.

$$m_L = -0.00047z + 2.66257$$

Equation 24. Resulting payload prediction equation.

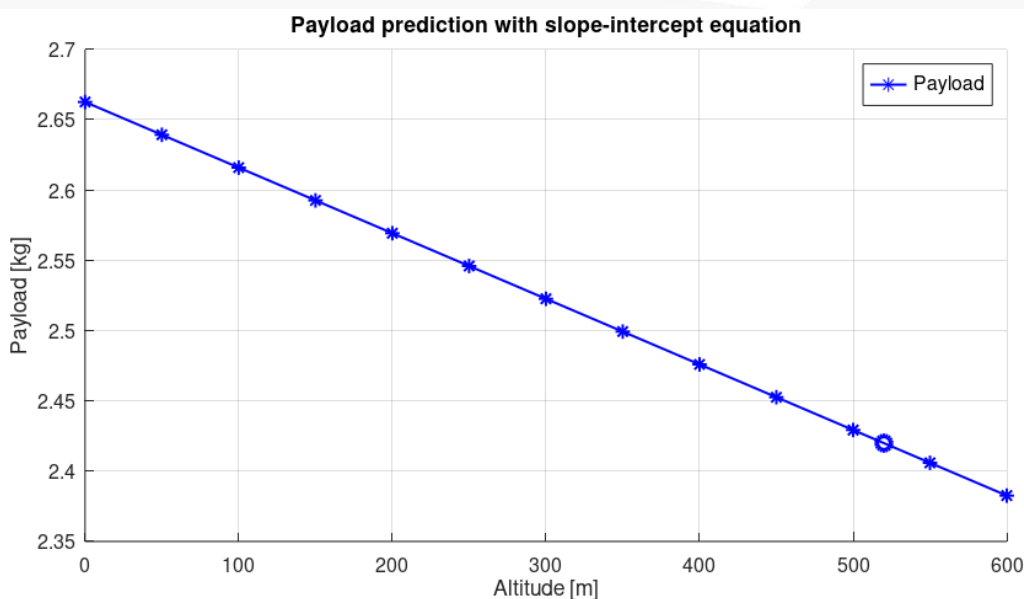


Figure 36. Payload mass prediction graph.

MANUFACTURING PROCESS

Different situations have made the manufacturing process difficult to begin, two main reasons were that the team was involved in another competition that required a lot of its resources (time, money and people the most) and the pandemic which did not allowed us to enter the University until November 2021. However, the team gained experience in creating bigger aircrafts of composite materials and wood, and with the recent event that required building a lot of prototypes in such a short time, the team is sure that the manufacturing process of Zotz will be a success.



Figure 37. U-FLY's past manufacture process. From left to right: a 4m span wing of carbon fiber; recovering a fuselage with Monokote; conventional tail empennage assembly.

For the wing two processes will be followed. For the carbon fiber central part, firstly a lower surface mold is machined in wood and the fiber gets prepared to be pasted on the mold. The same process is repeated for the upper surface and then both are pasted with an internal structure composed of airfoils, beams, and a wood leading and trailing edge. For the tips, the internal is essentially the same but using Monokote to recover the piece. The empennage follows the same procedure as the wooden part, and it also requires a jig to align the airfoils during the process. Lastly, the fuselage has a puzzle style where each part is laser cut and assembled like a puzzle piece, then it's pasted to one another and finally it's covered with Monokote. This process makes the manufacture so much easier and provides it with a resistant structure.

Despite that we can't offer images of this competition manufacture, we share the ones from our previous event as a proof of the team's capabilities and that we will manufacture the aircraft by ourselves.

OUTLOOK



Figure 38. Final model of Zotz.

Zotz is a very different aircraft from the ones who have developed. It made us research for a long time, attend multiple classes to comprehend new topics, do and re-do the design because it was still lacking something. In the end, as a team, we are all very glad this opportunity came to us as it allowed us to expand the limits of our regular work.

Although it is yet to be developed, we are capable of finishing the manufacture process, fulfill successful tests and prepare even more for the competition. As stated in the Gantt diagram in figure 3, a long way is awaiting us, but it'll happen in a split second.

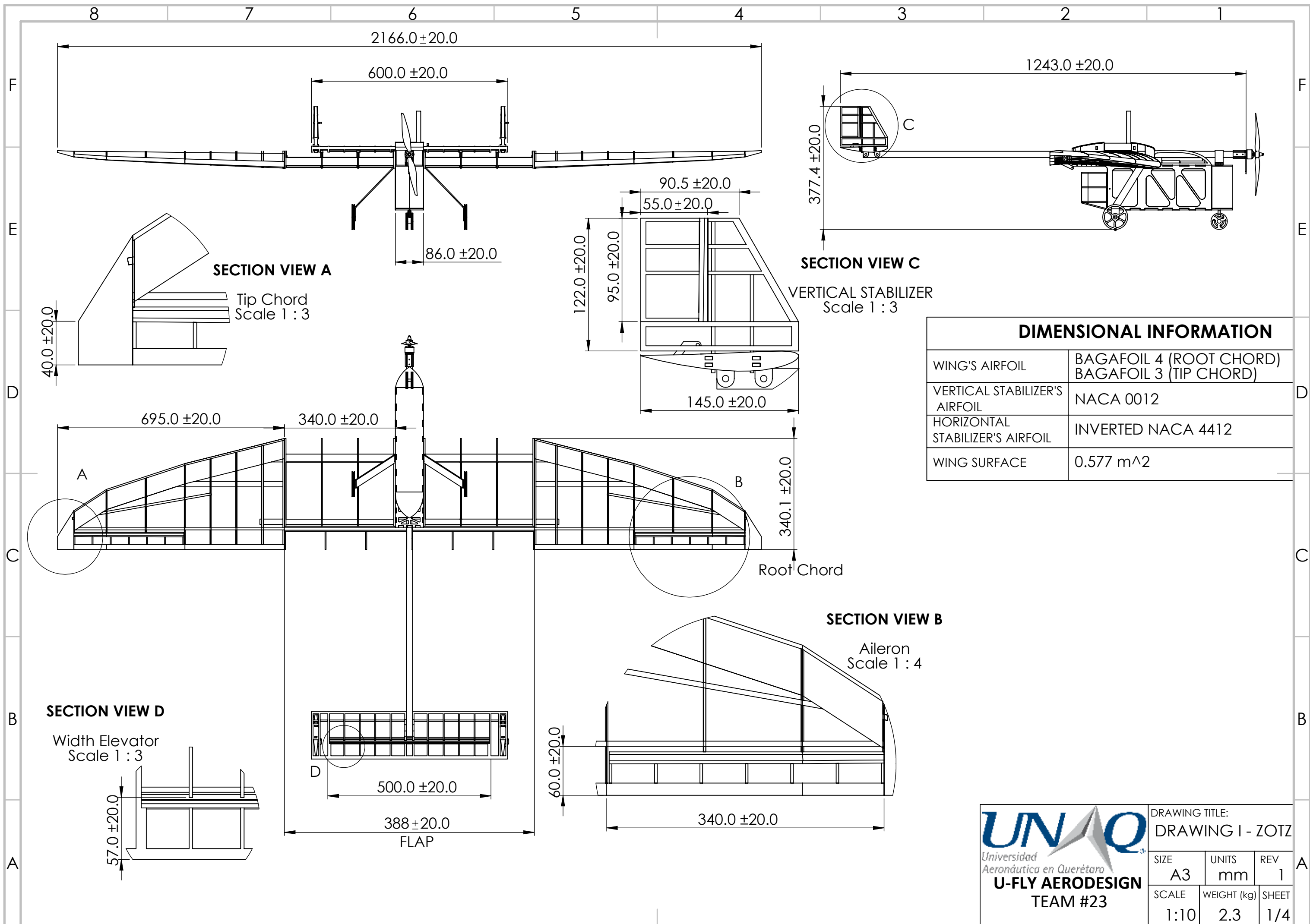
Its more important characteristics have been explained through these pages. Initially, the team analyzed the score system and decided which were the most important parameters to attack. As the payload, climb and distance were equally evaluated, the team decided not to neglect any of these attributes, but also concluded that the drag plays a key role in this competition, which was never the focus of the team before. After this, the ideas taken from previous experiences led to the use of the internal structure of the wing to carry more load and reducing the fuselage volume, therefore, reducing the drag. The empennage endured a very complicated labor as there were multiple changes in the aircraft that made this task very difficult on some occasions so that Zotz could accomplish its goal. The already selected propulsion system prompted to exercise new analysis to define the aircraft behavior. And the constant search of materials has made the team develop new strategies to acquire different products and manage them properly. One of the biggest problems was dealing with the empty weight, though, but the estimations set it around 2.3kg which is the goal of the manufacture process.

As shown, there were problems during the progression of the design, but the team found a way to solve each one of them. The outcome of this process is going to be an aircraft capable of carrying inside its whole structure 2.4kg of blood bags, climb about 80m and travel far distances at 18m/s in cruise flight. The tests and the hard work of the team will provide the ability to build the airplane in the shortest time possible, as well as load and unload it within two minutes with the whole stated payload. Zotz will be capable of satisfying this competition's requirements without doubt.

Since this is our first Air Cargo Challenge, the team has high expectations of it and our own performance, and we are sure that it will be a new beginning for the team.

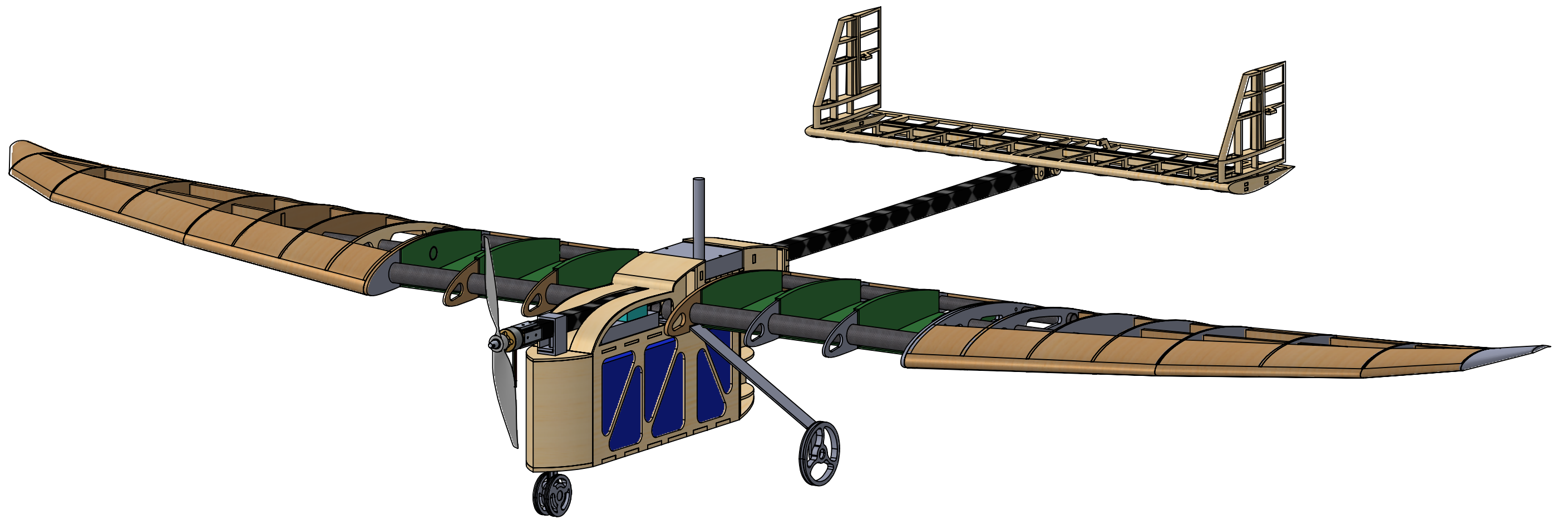
REFERENCES

- [1] D. P. Raymer, *Aircraft design: a conceptual approach*, 2nd ed., Washington, DC.: American Institute of Aeronautics and Astronautics, 1992.
- [2] S. Gudmundsson, *General Aviation Aircraft Design. Applied Methods and Procedures*, 2nd ed., Butterworth-Heinemann, 2022.
- [3] I. H. Abbot and A. E. von Doenhoff, *Theory of Wing Sections*, 2nd ed., Dover Publications, 1959.
- [4] P. D. Bravo Mosquera y A. Uribe Agudelo, *Diseño preliminar y conceptual de aeronave no tripulada para monitoreo de actividad volcánica*, Bogotá D.C.: Tesis de grado. Facultad de Ingeniería. Fundación Universitaria Los Libertadores., 2015.
- [5] J. S. Grass Nuñez, S. E. Rincón Ruíz y J. A. Roba, *Diseño conceptual y preliminar de una aeronave de categoría de transporte regional*, Bogotá D.C.: Tesis de grado. Facultad de Ingeniería. Fundación Universitaria Los Libertadores, 2017.
- [6] J. C. M. Morcillo, *Análisis, diseño y fabricación de un aeromodelo orientado a la maximización de la carga de pago para la competición Air Cargo Challenge*, Valencia: Tesis de grado. Escuela Técnica Superior De Ingeniería Del Diseño, Universitat Politècnica de València, 2021.
- [7] G. S. Señor, *Optimización Estructural y Aerodinámica de la plataforma alar de un avión UAV*, Madrid: Tesis de grado. Departamento de mecánica de medios continuos y teoría de estructuras. Universidad Carlos III de Madrid, 2016.
- [8] M. H. Sadraey, *Aircraft design: a systems engineering approach*, Chichester: Wiley, 2013..
- [9] R. C. Nelson, *Flight stability and automatic control*, 2nd ed., McGrawHill, 1998.
- [10] A. Kumar, M. A. Price y D. Riordan, *Theory and practice of aircraft performance*, Chichester: Wiley, 2016.
- [11] D. Doherty, «Analytical Modeling of Aircraft Wing Loads Using MATLAB and Symbolic Math Toolbo,» 2009. [En línea]. Available: <https://la.mathworks.com/company/newsletters/articles/analytical-modeling-of-aircraft-wing-loads-using-matlab-and-symbolic-math-tool>.
- [12] A. Herbert, "Pusher vs. Puller Propeller Aircraft Compared,," Airplane Academy., [Online]. Available: <https://airplaneacademy.com/pusher-vs-pullerpropeller-aircraft-compared/>.
- [13] L. E. Rodrigues, *Fundamentos da Engenharia Aeronáutica com Aplicações ao Projeto SAE-AeroDesign: Aerodinâmica e Desempenho.*, Salto: Edição do Autor, 2014.
- [14] M. H. Sadraey, *Aircraft Performance: An Engineering Approach.*, CRC Press., 2017.



DIMENSIONAL INFORMATION	
WING'S AIRFOIL	BAGAFOIL 4 (ROOT CHORD) BAGAFOIL 3 (TIP CHORD)
VERTICAL STABILIZER'S AIRFOIL	NACA 0012
HORIZONTAL STABILIZER'S AIRFOIL	INVERTED NACA 4412
WING SURFACE	0.577 m^2

 UNAQ Universidad Aeronáutica en Querétaro U-FLY AERODESIGN TEAM #23	DRAWING TITLE: DRAWING I - ZOTZ		
	SIZE A3	UNITS mm	REV 1
	SCALE 1:10	WEIGHT (kg) 2.3	SHEET 1/4

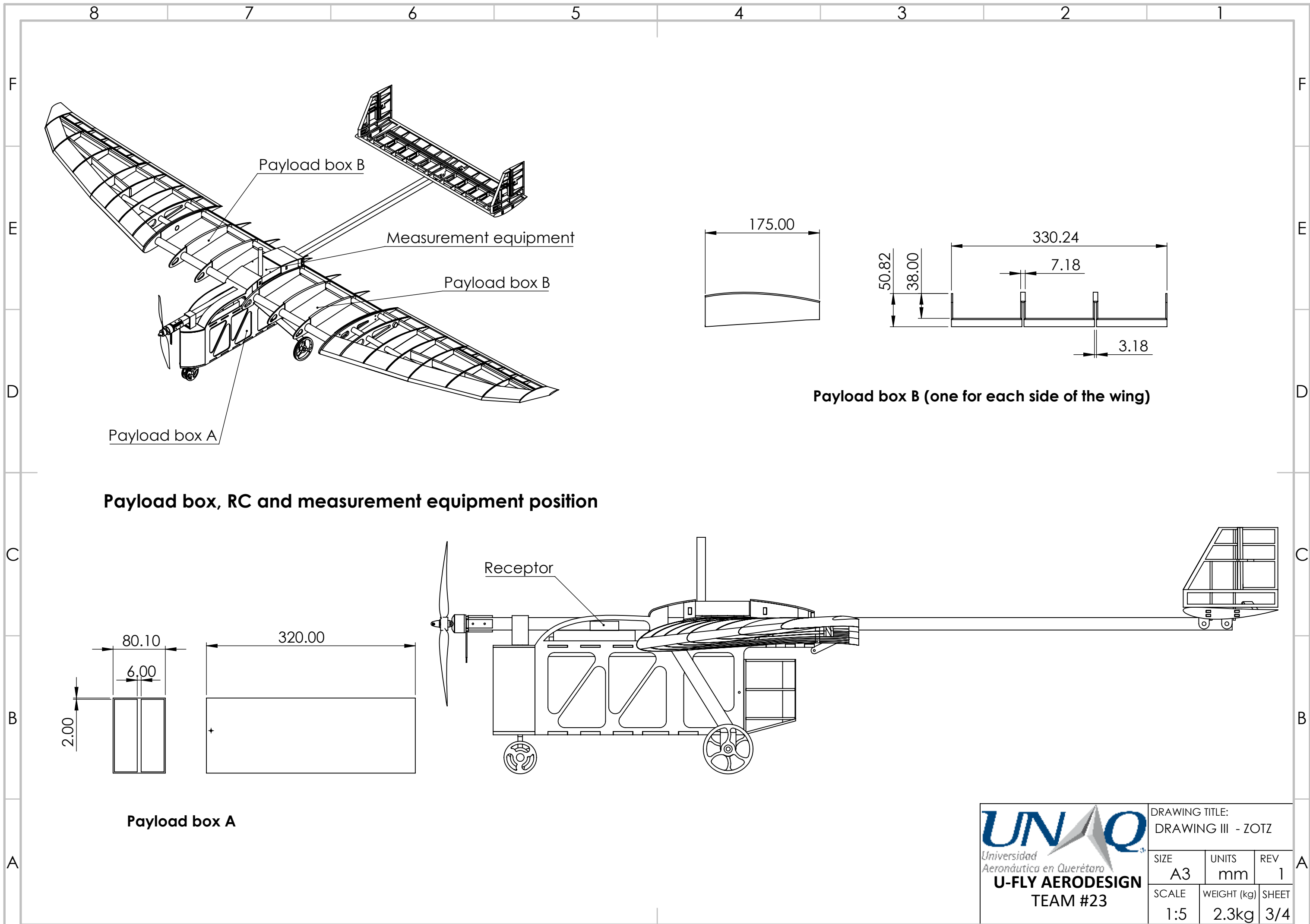


ISOMETRIC VIEW

ZOTZ AIRPLANE ASSEMBLY


 Universidad Aeronáutica en Querétaro
U-FLY AERODESIGN
 TEAM #23

DRAWING TITLE: DRAWING 2 - ZOTZ ISOMETRIC VIEW		
SIZE A3	UNITS mm	REV 1
SCALE 1:50	WEIGHT (kg) 2.3	SHEET 2/4



Payload box B
 Measurement equipment
 Payload box B
 Payload box A

Payload box B (one for each side of the wing)

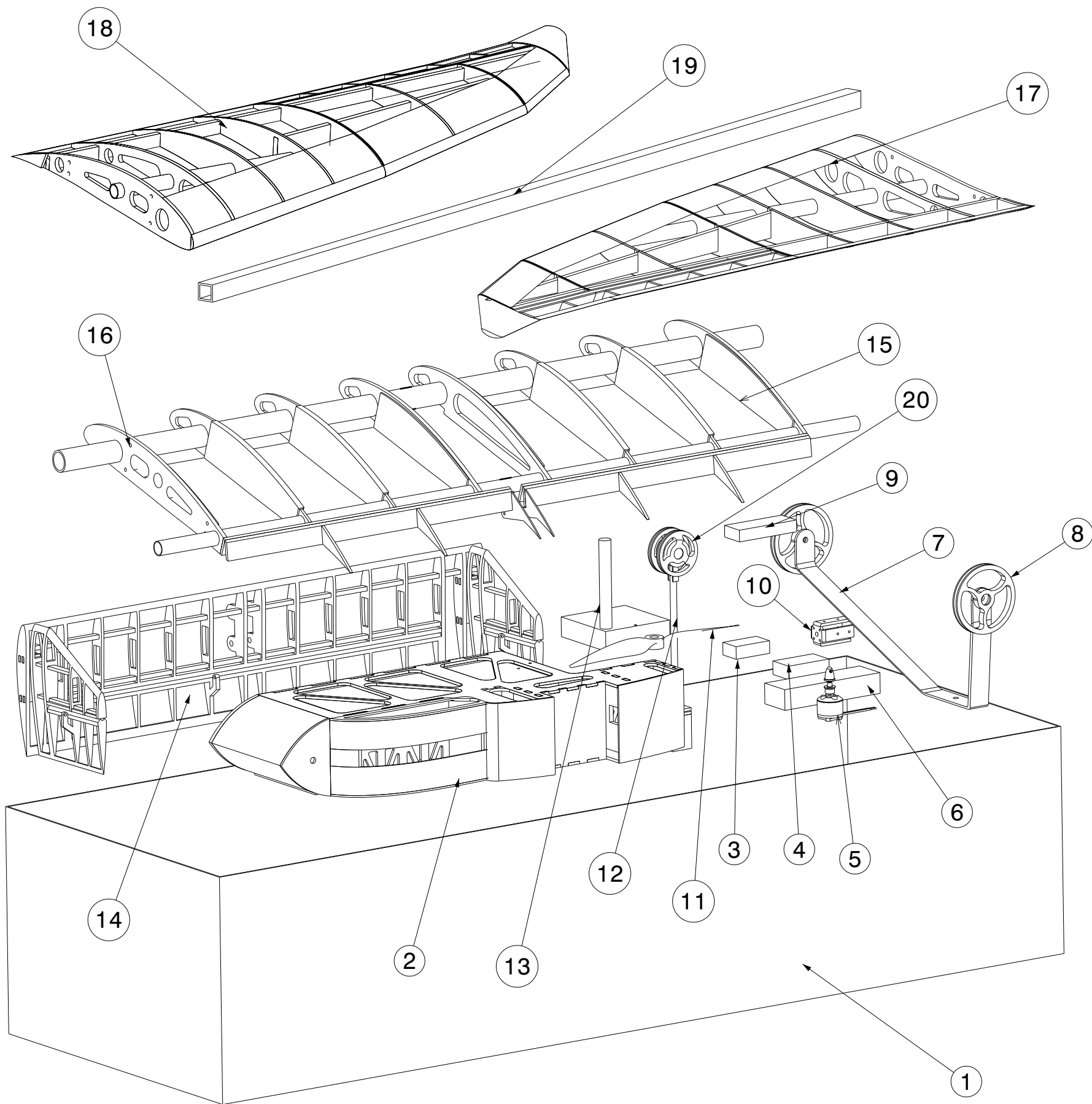
Payload box, RC and measurement equipment position

Receptor

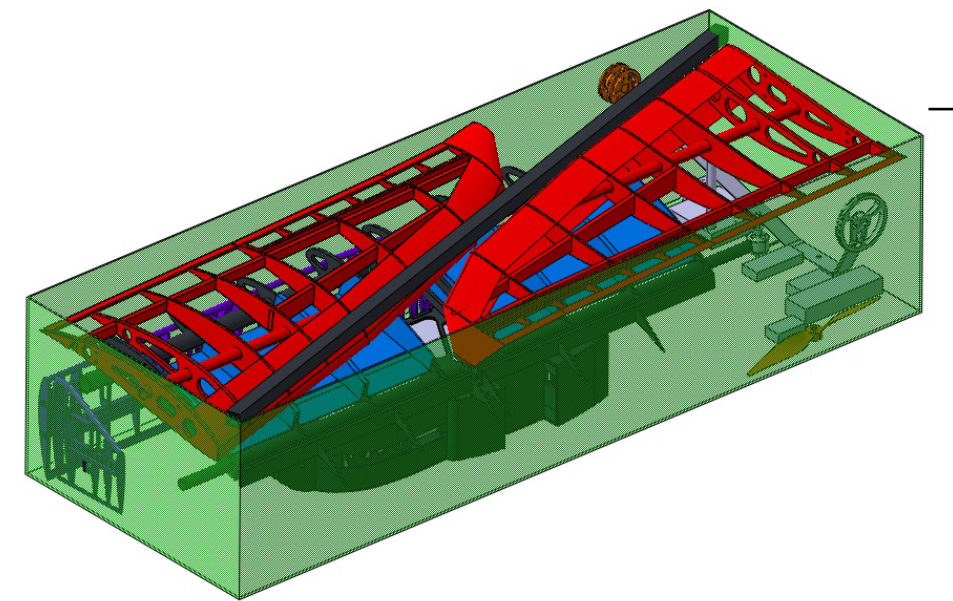
Payload box A

UNAQ
 Universidad Aeronáutica en Querétaro
U-FLY AERODESIGN
 TEAM #23

DRAWING TITLE: DRAWING III - ZOTZ		
SIZE A3	UNITS mm	REV 1
SCALE 1:5	WEIGHT (kg) 2.3kg	SHEET 3/4



ID	COMPONENT NAME	QUANTITY	MATERIAL
01	TRANSPORTATION BOX	1	NA
02	FUSELAGE/PAYLOAD BAY 1 STRUCTURE	2	WOOD/PLASTIC
03	SPEED CONTROLLER	1	NA
04	Li-Po AUX BATTERY	1	NA
05	ELECTRIC ENGINE	1	NA
06	Li-Po MAIN BATTERY	1	NA
07	MAIN LANDING GEAR	1	ALUMINIUM
08	PRINCIPAL WHEEL	2	ALUMINIUM
09	SIGNAL RECEPTOR	1	NA
10	ENGINE SUPPORT	1	ALUMINIUM
11	PROPELLER	1	PLASTIC
12	NOSE LANDING GEAR	1	ALUMINIUM
13	GPS LOGGER	1	NA
14	HORIZONTAL/VERTICAL STABILIZER STRUCTURE	1	WOOD/MONOKOTE
15	WING PAYLOAD BAY 2 STRUCTURE	1	PLASTIC
16	WING STRUCTURE	1	CARBON FIBER/WOOD/MONOKOTE
17	RIGHT WING TIP	1	WOOD/MONOKOTE
18	LEFT WING TIP	1	WOOD/MONOKOTE
19	PTR TUBE SUPPORT	1	CARBON FIBER
20	SECONDARY WHEEL	1	ALUMINIUM



REFERENCE PICTURE OF TRANSPORTATION BOX ASSEMBLY

EXPLODE VIEW
Isometric view
Scale: 1:5

			DRAWING TITLE: DRAWING IV - ZOTZ		
			SIZE A3	UNITS mm	REV 1
U-FLY AERODESIGN TEAM #23			SCALE 1:5	WEIGHT (kg) 2.3	SHEET 4/4